Chair of Drilling and Completion Engineering

Master's Thesis

Evaluating Uniaxial Compressive Strength of Cement by Applying Ultrasonic Measurement Technique

Paya Roknian

June 2021

PAYA ROKNIAN

Master Thesis supervised by
Prof. Kris Ravi
Prof. Mikhail Gelfgat

Evaluating Uniaxial Compressive Strength of Cement by Applying Ultrasonic Measurement Technique

dpe DEPARTMENT PETROLEUM ENGINEERING

MONTAN UNIVERSITÄT

Especially dedicated to Dr. Melika Hajkazemian;
who always encouraged and motivated me to set foot on this road.

MONTANUNIVERSITÄT LEOBEN
www.unileoben.ac.at

AFFIDAVIT

I declare on oath that I wrote this thesis independently, did not use other than the specified sources and aids, and did not otherwise use any unauthorized aids.

I declare that I have read, understood, and complied with the guidelines of the senate of the Montanuniversität Leoben for "Good Scientific Practice".

Furthermore, I declare that the electronic and printed version of the submitted thesis are identical, both, formally and with regard to content.

Date 16.06.2021

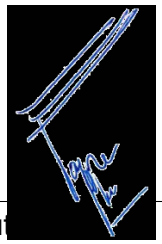

Signature Au
Paya Roknian

MONTANUNIVERSITÄT LEOBEN
www.unileoben.ac.at

Paya Roknian
OeAD-WVGmbH Josef-Heissl-Strasse 26
8700 Leoben

To the Dean of graduate Studies of the Montanuniversitaet Leoben

Declaration of Approval for the Digital Publication of Scientific Theses

I am aware that the thesis entitled "Evaluating Uniaxial Compressive Strength of Cement by Applying Ultrasonic Measurement Technique" will be subject to a plagiarism assessment and may be stored by Montanuniversität Leoben for an unlimited period of time.

I agree that the University Library of Montanuniversität Leoben may publish the thesis open access in the World Wide Web. For embargoed theses this will be done after the embargo expires.

Note: in case you refuse the open access publication in the World Wide Web, the thesis will only be published in printed form (after a possible embargo has expired) in the University Library (dissertations also in the Austrian National Library).

I hereby agree with the open access publication of my thesis on the World Wide Web:

☑ Yes

O No

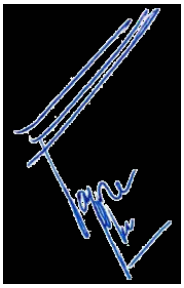

Date 16.06.2021

Signature Author

Abstract

Well integrity is one of the most important concepts in the upstream oil and gas industry. No matter whether a well is in drilling phase or has been already completed, the well integrity should be maintained. It is a multidisciplinary approach and has always been a serious challenge for major oil companies, regardless of operator or contractor. Therefore, all various departments in an oil company including drilling, completion, production, and plug and abandonment must cooperate and apply different methods, software and hardware, in order to maintain the well integrity for each operation of each section of each well.

This research work aims to perform ultrasonic measurement as a non-destructive evaluation method (NDE) to estimate the compressive strength of oil well cement with different densities and recipes at several ages. Therefore, the main project's target is to find a correlation between these two mechanical properties of oil well cement, the uniaxial compressive strength and the ultrasonic wave velocity, by inducing ultrasonic waves into the specific cement with unique composition at the known age. Using the correlation allows estimating the compressive strength of the cement in various densities and formulations other than the ones used in this project.

As to the methodology, six cement compositions with different recipes have been chosen for the linear measurement tests in which the ultrasonic wave velocity is correlated to the compressive strength of oil well cement. Additives used to prepare a wide density range from 11.0 to 16.0 ppg include barite, bentonite, and 3M glass bubble. Different regression methods have been tested only best, with the highest R^2 of 0.96 chosen to estimate the strength for 2D models. The factors considered in the model as input include water-to-cement ratio, density, ultrasonic wave velocity, and age.

The result shows that the composition with higher density, made by barite, is more resistant against being fractured and can convey an ultrasonic wave faster, while the lightweight cement, bentonite, and glass bubble made, has a lower compressive strength and a slower ultrasonic wave velocity. Moreover, a function model is created based on the correlations between compressive strength, ultrasonic wave velocity, age periods, and density. The model's inputs are ultrasonic wave velocity, age, and cement density, while the compressive strength is the model's output.

Moreover, by using the acquired data, different correlations among (UCS, density, age) and (UCS, UWV) and (UCS, age) and (UWV, age) have been shown all of which have accuracy above 0.96 R^2. Among the 2D correlations, UWV showed the best power fit for all cement samples. Eventually, by employing the 2D correlations and their generated coefficients, a rigorous analytical approach was given to define a generic 3D model of UCS as a transcendental function of several variables, including the density, age, and UWV. The function obtains the accuracy of R^2=0.77.

The modeling was a rigorous analytical approach. In case more data is generated in future work, the accuracy of the model can be improved. Another approach to improve the inherent accuracy could be employing machine learning techniques to get the best fit in transcendental functions rather than algebraic functions.

Zusammenfassung

Die Bohrlochintegrität ist eines der wichtigsten Konzepte in der vorgelagerten Öl- und Gasindustrie. Unabhängig davon, ob sich ein Bohrloch in der Bohrphase befindet oder bereits fertiggestellt wurde, sollte die Bohrlochintegrität aufrechterhalten werden. Dies ist ein multidisziplinärer Ansatz und war schon immer eine ernsthafte Herausforderung für große Ölgesellschaften, unabhängig vom Betreiber oder Auftragnehmer. Daher müssen alle verschiedenen Abteilungen eines Ölunternehmens, einschließlich Bohrung, Fertigstellung, Produktion und Plug and Abandonment, zusammenarbeiten und verschiedene Methoden, Software und Hardware anwenden, um die Bohrlochintegrität für jeden Betrieb jedes Abschnitts jedes Bohrlochs zu erhalten.

Diese Forschungsarbeit zielt darauf ab, Ultraschallmessungen als zerstörungsfreie Bewertungsmethode (NDE) durchzuführen, um die Druckfestigkeit von Beton mit unterschiedlichen Dichten und Rezepturen in verschiedenen Altersstufen abzuschätzen. Daher ist das Hauptziel des Projekts, eine Korrelation zwischen diesen beiden mechanischen Eigenschaften des Betons, der einachsigen Druckfestigkeit und der Ultraschallwellengeschwindigkeit zu finden, indem Ultraschallwellen in den spezifischen Beton mit einzigartiger Zusammensetzung bei bekanntem Alter eingeleitet werden. Die Verwendung der Korrelation ermöglicht die Abschätzung der Druckfestigkeit des Betons in verschiedenen Dichten und Rezepturen, die nicht in diesem Projekt verwendet wurden.

Was die Methodik betrifft, so wurden sechs Zementzusammensetzungen mit unterschiedlichen Rezepturen für die linearen Messversuche ausgewählt, bei denen die Ultraschallwellengeschwindigkeit mit der Druckfestigkeit des Betons korreliert wird. Um einen breiten Dichtebereich von 11,0 bis 16,0 ppg vorzubereiten, wurden Zusatzstoffe wie Schwerspat, Bentonit und 3M-Glasblase verwendet. Es wurden verschiedene Regressionsmethoden getestet, wobei das höchste R^2 von 0,96 für die Schätzung der Festigkeit für 2D-Modelle gewählt wurde. Zu den Faktoren, die in dem Modell als Eingabe berücksichtigt wurden, gehören das Wasser-Zement-Verhältnis, die Dichte, die Ultraschallwellengeschwindigkeit und das Alter.

Das Ergebnis zeigt, dass die aus Schwerspat hergestellte Zusammensetzung mit höherer Dichte widerstandsfähiger ist und eine Ultraschallwelle schneller übertragen kann, während der aus Bentonit und Glasblasen hergestellte Leichtzementbeton eine geringere Druckfestigkeit und eine langsamere Ultraschallwellengeschwindigkeit aufweist. Außerdem wird ein Funktionsmodell erstellt, das auf den Korrelationen zwischen Druckfestigkeit, Ultraschallwellengeschwindigkeit, Altersperioden und Dichte basiert. Die Eingaben des Modells sind Ultraschallwellengeschwindigkeit, Alter und Betondichte, während die Druckfestigkeit die Ausgabe des Modells ist.

Darüber hinaus wurden unter Verwendung der erfassten Daten verschiedene Korrelationen zwischen (UCS, Dichte, Alter) und (UCS, UWV) und (UCS, Alter) und (UWV, Alter) gezeigt, die alle eine Genauigkeit von über 0,96 R^2 aufweisen. Unter den 2D-Korrelationen zeigte UWV die beste Leistungsanpassung für alle Zementproben. Schließlich wurde durch die Verwendung der 2D-Korrelationen und ihrer generierten Koeffizienten ein strenger analytischer Ansatz gegeben, um ein generisches 3D-Modell der UCS als transzendente Funktion mehrerer Variablen, einschließlich der Dichte, des Alters und der UWV, zu definieren. Die Funktion erhält eine Genauigkeit von R^2=0,77.

Die Modellierung war ein strenger analytischer Ansatz. Falls in zukünftigen Arbeiten mehr Daten generiert werden, kann die Genauigkeit des Modells verbessert werden. Ein weiterer Ansatz zur Verbesserung der inhärenten Genauigkeit könnte die Verwendung von Techniken des maschinellen Lernens sein, um die beste Anpassung in transzendenten Funktionen anstelle von algebraischen Funktionen zu erhalten.

Acknowledgements

I would like to express my sincere appreciation to my supervisors, Professor Mikhail Gelfgat, for his unconditional supports and thoughtful feedbacks not only during the master thesis, but also in the whole program. Besides, Professor Kris Ravi, who gave me the opportunity to perform this project; his remarks and engagements have been undoubtedly valuable. Without their persistent guidance, the goal of the project would never have been reached.

Special thanks to my co-supervisor, Dipl. –Ing. Arash Nasiri. He has always been responsive and helpful to my enormous doubts, questions, and emails regardless of time. He has technically and scientifically helped and supported me a lot. Thank you, Arash!

I appreciate Dipl. –Ing. Abdelfattah Lamik for his supports and guidance as co-supervisor.

I am grateful to Well Integrity Platform members, specially Ass. Prof. Dipl. –Ing. Dr.mont. Michael Prohaska as WIP's deputy managing director, who provided necessary equipment and a friendly environment that helped me to perform the thesis with a peaceful mind and the best possible quality.

I am also thankful to all scientific and administrative members of DPE, specially Alexander Fine, Patrizia Gäbler, and Bettina Matzer, who has been always helpful and cooperative to complete this project.

Thanks to Ronald Heijnen, Key Account Manager of 3M company for providing 3M Glass Bubble for enhanced lightweight slurry.

Last but not least, I would like to express my gratitude to the most important people in my life, my family: Nasrin and Saeed, my parents, and Pooya, my brother. Thanks for your unconditioned love and unfailing supports throughout my years of study.

Contents

Chapter 1 Introduction

1.1 Project Description

An oil and gas well is a complex structure that contains a variety of natural and artificial objects. Natural objects are like the earth, fluid, rocks, etc., which usually have unpredictable behavior. On the other hand, artificial objects are designed and made based on calculation and engineering, such as casing, cement, and mud. Well integrity is one of the main significant objectives that should be considered, reached, and maintained during the lifecycle of oil and gas wells. It does not only belong to a specific phase like drilling but must be regarded for each activity in all the well design, construction, completion, production, and abandonment phases.

This study aims to find a practical and reliable way to determine cement quality behind the casing by ultrasonic measurement. One of the most important cement properties that should be monitored and measured in order to assess its quality is uniaxial compressive strength. Measuring the compressive strength of the cement by ultrasonic provides an opportunity to test the cement without breaking it. This study includes preparing different cement samples, exposing the samples to the ultrasonic waves, performing the uniaxial compressive strength test, and finding a correlation of uniaxial compressive strength with ultrasonic measurement of any cement sample.

This study aims to find a generic empirical correlation between the ultrasonic wave velocity and compressive strength of standard cubic and cylindrical cement plugs from cement class G. Here we have only focused on the linear ultrasonic testing and a regression technique of 0.95 considering the water to cement ratio, heavy weight and light weight additives to cement ratio, slurry density, age of curing and amount of cement as independent variables. A correcting factor is also added to the correlation that considers the effect of the shape of the samples.

1.2 Thesis Structure

In general, this thesis consists of two main parts:

- Theoretical part
- Practical part

The theoretical part includes reviewing the literature, studying the principle of ultrasonic wave measurement and its fundamental methods, how to apply these methods in order to get the most precise result and mitigate errors, finding the procedure of making cement slurries with different densities, application of uniaxial compressive strength test to each specimen, validating and verifying the laboratory outputs and ultrasonic measurements, and how to extract and find the most suitable correlation factor/equation between compressive strength and ultrasonic wave velocity.

The practical part is performed in the fluid laboratory of the department petroleum engineering of Montanuniversität Leoben. Six main categories of cement samples were

prepared and compared. The standard slurry (44% of W/C ratio with no additive), the enhanced lightened slurry (with 3M glass additive), the heavy weight slurry (3 and 6% of barite), the lightweight slurry (0.8 and 2% of bentonite as additive). Once samples are prepared (in cubical and spherical shapes) the ultrasonic wave velocity is measured by the oscillator. The next step is to execute the destructive test and measure each sample's uniaxial compressive strength with specific density for both cubical and cylindrical shapes. Each step will be further discussed in the following chapters.

1.3 Thesis Objective

The purpose of the master thesis is to find a correlation between uniaxial compressive strength and measurement-wave velocity of oil well cement samples of cement class G. We kept the cement class constant because of the importance of class G in oil and gas industry (Park et al., 2019). Correlation is a bivariate analysis that measures the strength of association between two variables and the direction of the relationship. In statistics, the correlation coefficient is a measure that determines the degree to which two variables' movements are associated. In other words, the project's final target is to acquire a numerical relationship between the uniaxial compressive strength of the different cement densities with induced ultrasonic waves in order to estimate the strength of cement samples of known age and composition by measuring the ultrasonic wave velocity. The correlation is calculated as a result of comparing the uniaxial compressive strength test and ultrasonic measurement outputs found and mentioned in the practical step.

1.4 The Importance of the Study

Evaluation of the cement behind the casing has always been a challenge. Cement sheath is one of the most critical elements of the well barrier, and its quality plays a significant role in avoiding any danger and risk in the downhole and the surface. As time negatively affects cement quality, cement conditions should be monitored and evaluated during a well life cycle. As the production phase is the longest phase in the lifecycle of a well, it is vital to check the cement condition at this phase.

This study provides a solution to identify, evaluate, and monitor the cement condition behind the casing without damaging it by using ultrasonic waves. Besides, the result would probably be applicable in the industry. Measuring the compressive strength of cement behind the casing in actual wells, inducing ultrasonic waves, and comparing the outcome with a correlation factor/equation, as a result of this study, could help identify the quality of the placed cement. Thus, more precise decisions could be taken for performing well remedial treatment or plug and abandonment.

Chapter 2 Literature Review

The chapter aims to present the reader with a background on the concepts participating in the theoretical and practical parts of the thesis being used by the author.

2.1 Well Barrier

Well barrier is a critical concept in well integrity. According to Norsok D-010 Standard, the well barriers are a set of envelopes including one or more dependent well barrier elements which should prevent unintentional flowing of hydrocarbon from a formation to another formation or the surface (2004). A well barrier element, WBE, is a mechanical and/or physical object naturally or artificially placed in the wellbore or at the surface to prevent or stop the uncontrolled fluid flow (Vignes, 2011). Norsok D-010 standard classifies well barriers into two types:

- Primary well barriers:
- Secondary well barriers:

Each specific phase in an oil and gas well's lifecycle has its well barrier design. It means that the well barriers in the drilling phase would not be the same as those used in production or abandonment phases, although there would be some common well barriers.

The independence of primary and secondary well barriers is essential. These two should not have any common well barriers elements. If a common well barrier exists, then one of them should be able to shear any tools that go through the well barrier, seal the wellbore after shearing, and seal the wellbore with any size tools that pass the well barrier.

If there is a risk of uncontrolled flow in the wellbore between formation zones due to differential pressure, one well barrier shall be in place all during well activities. While in case of any risk of unintentional flow from the borehole to the external environment, there shall be two well barriers available during well activities. Based on Norsok D-010, this rule is applicable even for suspended or abandoned wells.

In addition, well barrier elements shall be verifiable. After placing the WBE in its designated position, its integrity and function must be verified. The verification includes the function and leak test, which applies differential pressure against the element.

An example of WBE in drilling, coring, or tripping activities is shown in Figure 1 (Norsok D-010, 2004). Fluid column, as a primary well barrier, is illustrated in blue color, and five different secondary well barriers containing casing cement, casing, wellhead, high-pressure riser, and blowout preventer are represented in red color:

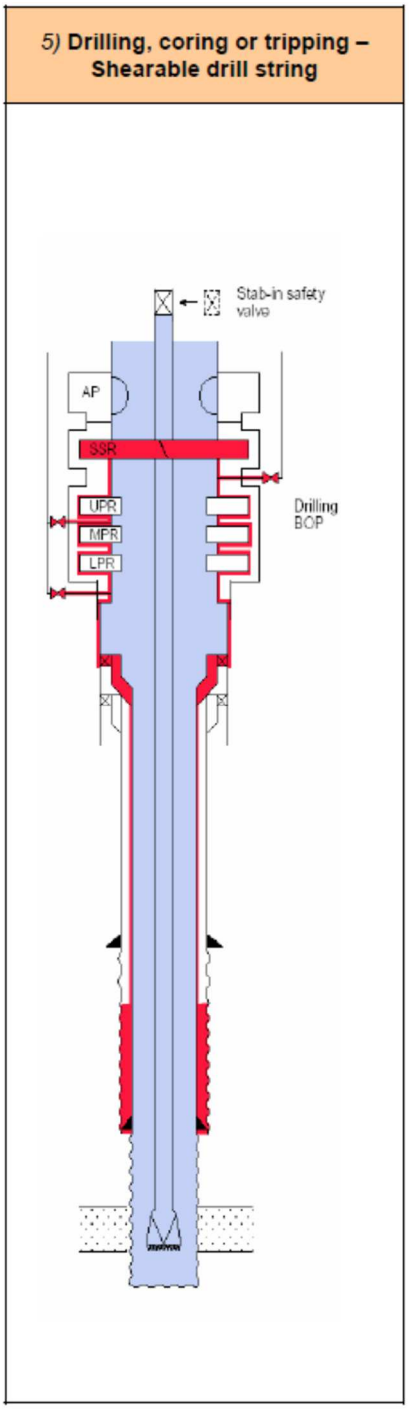

Figure 1 - WBE in Drilling

2.2 Portland Cement

Cement sheath is a physical layer placed between casing and formation and used as a well barrier element. It has three main functions:

- hold casing in place
- prevent fluid migration between formations
- protect the casing from corrosion (Pankaj Munjal et al., 2019)

The most known and applicable cementitious material in the upstream oil and gas industry is Portland cement. It usually originates from limestone. It is a fine powder produced by heating limestone and clay minerals in a kiln to form a clinker, which is the main component of Portland cement. It is produced by heating an ensemble of limestone with silica, alumina, iron oxide-containing materials (L. Ferrari et al., 2012), grinding the clinker, and adding 2 to 3 percent of gypsum (Courland, 2011). Portland cement is a type of hydraulic cement that sets and develops compressive strength due to hydration and chemical reactions between water and the cement's existing compounds (Nelson et al., 2006).

Characterization of Portland cement properties is based on the mineralogical compositions of the clinker. Table 1 shows the mineralogical compositions of the Portland cement clinker (Nelson et al., 2006).

Oxide Composition	Cement Notation	Common Name	Concentration (wt%)
$3CaO.SiO_2$	C_3S	Alite	55-65
$2CaO.SiO_2$	C_2S	Belite	15-25
$3CaO.Al_2O_3$	C_3A	Aluminate	8-14
$4CaO.Al_2O_3.Fe_2O_3$	C_4AF	Ferrite phase	8-12

Table 1 - Mineralogical Composition of Portland Cement Clinker

American Petroleum Institute (API) is an association that establishes and maintains standards for the oil and gas industry. It specifies the cement into six classes (A, B, C, D, G, and H) and three grades, including ordinary (O), moderate sulfate resistant (MSR), and high sulfate resistant (HSR) in API 10A, 24th edition published December 2011.

Cement Class A: This cement class is designed to use from surface to 6,000 ft depth. Class A is available in O grade and used when no special properties are required.

Cement Class B: Same as class A, this class is also applicable at a maximum depth of 6,000 ft from the surface. In contrary to class A, this class is available in both MSR and HSR grades.

Cement Class C: It is called high early strength cement and used in the same depth as the first two classes, 6,000 ft from the surface. As required in high early strength conditions, this cement is available in all three grades, O, MSR, and HSR.

Cement Class D: Instead of surface, this class is intended to use 6,000 ft to 10,000 ft depth. Under conditions of moderately high pressure and temperature, this class is being used. Class D is available in both MSR and HSR grades.

Cement Class G: This class is using as a basic well cement. During this class's manufacture, no additives other than water or calcium sulfate, or both, are allowed to be blended with the clinker. It is possible to use class G from the surface up to 8,000 ft. Same as class D, this class is also available in both MSR and HSR grades.

Cement Class H: This class has a similar composition with class G, and the only difference is that class H is coarser than class G. In terms of grades and the maximum depth of application, the class is the same as class G.

Among these six cement classes, class G and class H are the most usable ones in the oil industry. In other words, more than 95% of international services companies use cement class G, while it is almost 80% of class G and H in the United States (Guner et al., 2017). Due to this fact, the cement which is used in this study is class G.

2.3 Compressive Strength

Compressive strength is one of the most important mechanical properties of cement that illuminates the slurry's mechanical characteristics. The other mechanical properties are including flexural strength, tensile splitting strength, and modulus of elasticity (Bahij et al., 2020). The compressive strength of a cement sample is its capability to withstand compressive load before being fractured. Generally, the compressive strength is defined as the maximum compressive load divided by its cross-sectional area (Bahij et al., 2020) and calculated by (Equation 1):

$$\sigma = \frac{F}{A}$$

(Equation 1)

Where σ is compressive strength [N/mm^2 or MPa],

F is applied load [N],

A is the cross-sectional area [mm^2].

Strain is another important parameter that should be measured to calculate the compressive strength. In general, the measure of any stretch or deformation of an object owing to an applying force is called strain (EN 380 US Naval Academy Course). It is a dimensionless parameter that is calculated by dividing the length of change by the initial length of the sample (Equation 2):

$$\varepsilon = \frac{l_f - l_i}{l_i}$$

(Equation 2)

Where ε is strain [dimensionless, shown in percentage],

l_f is the final length after applying force [mm],

l_i is the initial length before performing the test [mm].

2.3.1 Stress-Strain Curve

Plotting the stress-strain curve is necessary to find any solid sample's compressive strength, including cement. The stress-strain curve is the output of an unconfined compressive strength test equipment. It is a two axes plot that shows the compressive stress on the y-axis, and the strain on the x-axis (Figure 2) (EN 380 US Naval Academy Course):

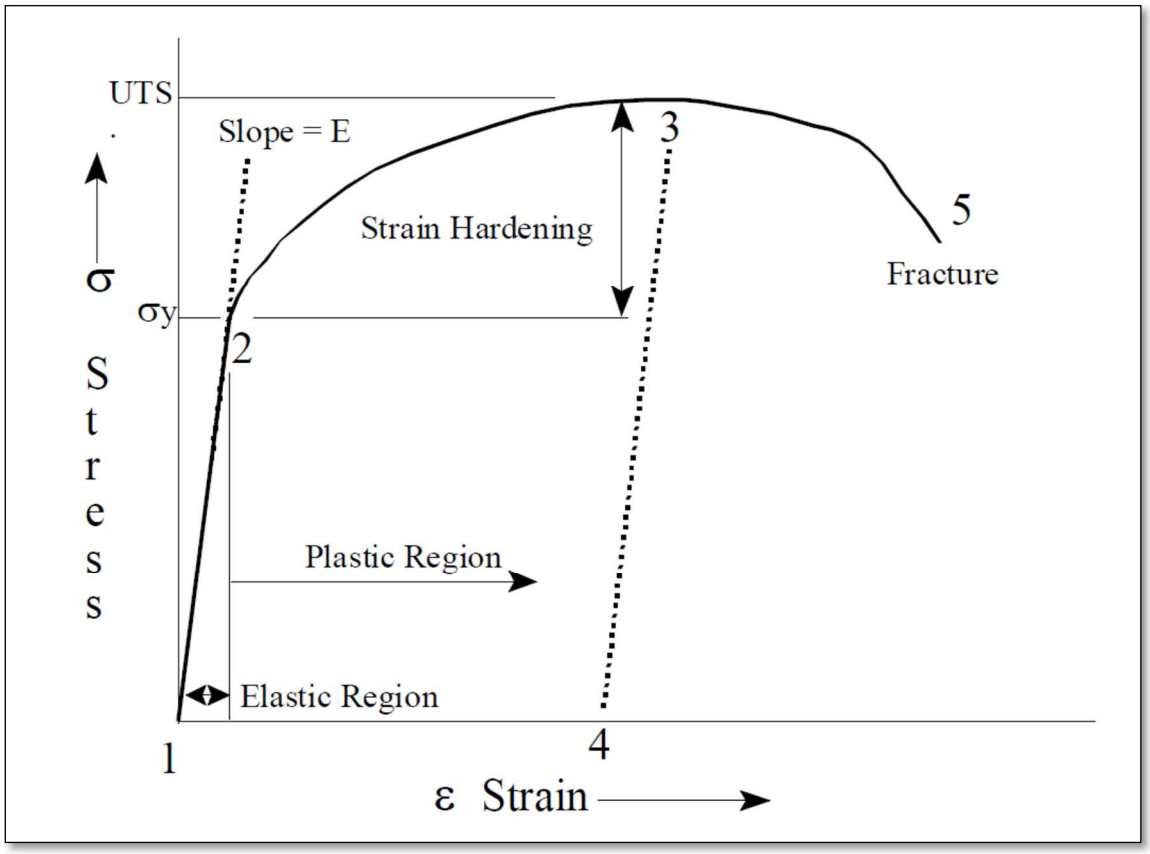

Figure 2 - Stress-Strain Curve (EN 380 US Naval Academy Course)

Refer to Figure 2, where the stress-strain curve is divided into various regions by five different points. There is no load applied to the sample at point one to keep its original shape without deformation. By applying the load to the sample, both stress and strain increase from point one to point two with the same proportion. This ratio, which is calculated from dividing stress by strain, is called Elastic or Young's Modulus (Equation 3). Therefore, the limited region between points one and two is called the Elastic region. If the sample is unloaded before reaching point two, then the curve would back down to point one, representing the sample's original shape.

$$E = \frac{\sigma}{\varepsilon}$$

(Equation 3)

Where E represents young modulus [N/mm^2 or MPa],

σ is compressive strength taken from (Equation 1)[N/mm^2 or MPa],

And ε illustrates the strain mentioned in equation 2 [dimensionless, shown in percentage].

If the load is high enough to pass point two, the sample will never back to its original form. This point is called Yield Strength. At this point, the sample has already been deformed permanently. Hence, the region beyond point two is named the plastic region.

As shown in Figure 2, deformation increases by applying more stress to the sample. However, the rate is not the same as the elastic region. Point three is called the

Compressive Strength meaning that if the sample is strained beyond this value, the stress decreases as non-uniform deformation and necking occurs. If the sample is reached to point five, it will be fractured.

If the load is removed from the sample at any point between point two and point three, the compressive stress, but not the strain, is zero. It is what the figure is showing at point four. The reason that the strain is not zero is because of the permanent deformation which was described before. If the sample is loaded at point four again, the compressive strength starts to reach the yield strength like the young's modulus. While young's modulus is always unchanged, the yield strength will be increasing due to permanently straining the sample. Permanently straining the material in order to increase the yield strength is called Strain Hardening (EN380 US Naval Academy Course).

2.4 Ultrasonic Measurement

Nowadays, ultrasonic has become one of the primary methods for advanced monitoring and diagnostics of material life estimation and quality that provides real-time detection and makes instant necessary decisions (Ensminger et al., 2012). Therefore, it is also applicable for evaluating the cement sheath quality behind the casing without destruction and fracture on the cement.

Also, the ultrasonic measurement can be classified as a Non-Destructive Test (NDT). NDT is generally defined as an examination, test, or evaluation performed on any test object without changing or altering the object that may have an effect on the object's performance, usability, and usefulness (Basrawi et al., 2003).

2.4.1 Principle

As a branch of acoustics, ultrasonic deal with vibratory waves in solids, liquids, and gases at frequencies above 20 kHz (20,000 cycles per second), the hearing range frequency of a young person (Ensminger et al., 2012). As ultrasonic waves are mechanical waves, they cannot exist and transmit through the vacuum, but only within mass media. It means the energy stored in ultrasonic waves can be transferred from one mass or any material element by direct and intimate contact between masses or elements (Pain, 1999). In solid materials, the propagation properties depend on the elastic properties of the medium. Compression, shear, surface, and interface vibrations are some forms of ultrasonic waves in solid mediums (Ensminger et al., 2012).

In many respects, ultrasonic can be considered similar to light or an electromagnetic wave (Pain, 1999). Ultrasonic is a form of mechanical energy, and ultrasonic waves travel through a medium at a velocity that is dependent on the properties of the medium. Similar to light, ultrasound is reflected from surfaces, refracted when going from one medium into another, which affects change in sound velocity and diffracted at the edges of surfaces or around obstacles (Ensminger et al., 2012).

Suppose the stresses developed in the ultrasonic waves remain in the linear and elastic range of the medium. In that case, the particle motion is sinusoidal at any point in an ultrasonic wave with a certain frequency.

2.4.2 Wave Propagation

In general, a wave is a disturbance from point to point that carries energy with no amount of mass transfer. The effect of spreading a local perturbation in a medium is referred to as wave propagation. The vibration of atoms and molecules at the material makes the sound propagate in elastic bodies. Sound propagation's velocity depends on the mechanical characteristics of the body's materials (Ultrasonic Nondestructive Evaluation Systems, 2015). Wave propagation in a medium causes reduction or amplitude attenuation (Ensminger et al., 2012).

The compressibility of a medium is the reason for sound wave propagation. Sounds waves are classified as below by frequency:

- Infrasound waves – below 20 Hz
- Acoustic waves – between 20 Hz to 20 kHz
- Ultrasonic waves – more than 20 kHz

On the other hand, considering the particle oscillation direction concerning propagation direction, sound waves are identified as three types:

- Longitudinal waves
- Shear waves
- Surface waves (Szabo TL et al., 2000)

Longitudinal Waves: if the particle oscillation is in the same direction as the wave propagation, the wave is called longitudinal (Figure 3). Longitudinal waves are also called pressure traction waves and are shown as P-waves. These waves can propagate in solids, liquids, and gaseous materials.

P-waves speed propagation can be calculated from (Equation 4) as below:

$$v_p = \sqrt{\frac{E_d(1-\nu_d)}{\rho(1+\nu_d)(1-2\nu_d)}}$$

(Equation 4)

Where v_p is P-wave velocity [m/s],

E_d is young's modulus [MPa],

ν_d is Poisson's ratio,

And ρ is density [kg/m^3].

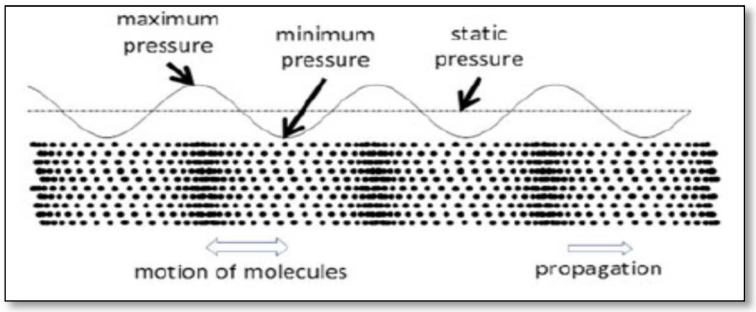

Figure 3 - Longitudinal Waves (Ultrasonic Nondestructive Evaluation Systems, 2015)

Shear Waves: or S-waves, when the particles oscillate perpendicular to wave propagation, shown in Figure 4. S-waves are relatively weaker than longitudinal waves, and in contrast to P-waves, they are not effectively propagated in liquid and gaseous materials. Therefore, shear waves are generally using part of the longitudinal waves' energy to be generated.

(Equation 5) illustrates the speed propagation of S-waves:

$$v_s = \sqrt{\frac{E_d}{2\rho(1+\nu_d)}}$$

(Equation 5)

Where v_s is S-wave velocity [m/s],

E_d is young's modulus [MPa],

ν_d is Poisson's ratio,

And ρ is density [kg/m^3].

And the rest of the parameters and units used in the S-waves equation are the same as equation 6.

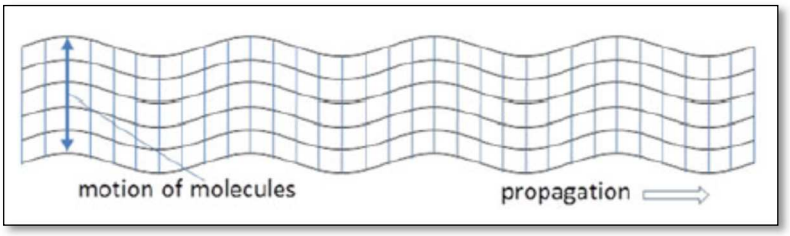

Figure 4 - Shear Waves (Ultrasonic Nondestructive Evaluation Systems, 2015)

Surface Waves: the usage of surface waves is exceptional and rare compared to longitudinal and shear waves. This wave propagates due to surface layers' effects and is slightly slower than shear waves. The speed of the surface wave is calculated by Bergmann's formula shown as (Equation 6) (Bergmann L, 1957):

$$v_p = \frac{0.87 + 1.12\nu_d}{1+\nu_d}\sqrt{\frac{E_d}{2\rho(1+\nu_d)}}$$

(Equation 6)

Where v_p is surface wave velocity [m/s], and all units and parameters are the same as equation 6 (Ultrasonic Nondestructive Evaluation Systems, 2015).

2.4.3 Linear and Non-Linear Ultrasonic Testing

The interaction between tested media and ultrasonic waves can be linear or non-linear (Ensminger et al., 2012). Both linear and non-linear ultrasonic testing have been used for material mechanical characterization and non-destructive evaluation tests.

Linear ultrasonic testing is primarily applied for evaluating material properties (Li et al., 2013). At this testing method, an object receives high-frequency sound waves. Traveling through the material and colliding with the edge of holes lead the waves to be reflected, diffracted, attenuated, and finally defected at the back of the object. Then, the transmitted (pitch-catch) or reflected wave (pulse-echo) can be analyzed (Haller, 2007). In fact, the linear testing measures the ultrasonic velocity and attenuation (Jianfeng Zhang et al., 2014). The advantages of linear testing are finding the defect or discontinuity on the material and the object's thickness (Haller, 2007). But there are some problems with this testing. First of all, linear testing is not sensitive to microstructural changes. It cannot detect the discontinuities or fractures greater than the wavelength of the ultrasonic wave (Mostavi et al., 2017). As a matter of fact, half of the ultrasonic wavelength is the smallest size for detecting a defect.

Another problem is that the defects parallel to the wave's direction of the motion are rarely investigated. Moreover, the surface's roughness can negatively affect the result (Haller, 2007). Ultrasonic Compressional Wave Velocity (UPV) and Resonance Ultrasound Spectroscopy (RUS) are categorized as linear ultrasonic testing techniques (Shokouhi et al., 2017).

On the other hand, non-linear testing has shown a promising capability to discover microstructural damages in a wide range of materials including oil well cement (Shokouhi et al., 2017). In this technique, an object is exposed to a single frequency wave by a piezoelectric transducer. The wave travels through the object, which is a nonlinear medium and another piezoelectric element receives the wave. The frequency of the received wave is presented and shown by a device such as an oscilloscope. A typical setup of this technique is shown in Figure 5.

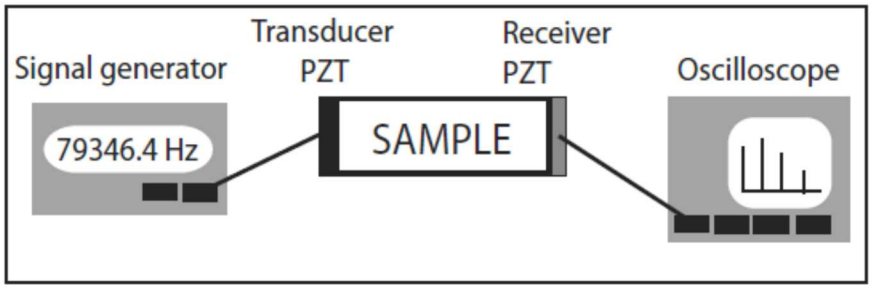

Figure 5 - Typical Setup for Non-linear Ultrasonic Testing (Haller, 2007)

As shown in Figure 6, at x=0, the initial wave is sent to the object. The wave has become distorted by passing the path from point zero to "a". The same phenomena with more distortion happen at point "b". All changing in frequency is interpreted as non-linearity indicator and damage detection (Haller, 2007). One of the most advanced techniques in non-linear ultrasonic is Dynamic Acousto-Elastic Testing (DAET). In addition, Non-linear Resonance Ultrasound Spectroscopy (NRUS) is another popular technique in the field of non-linear ultrasonic testing (Shokouhi et al., 20017).

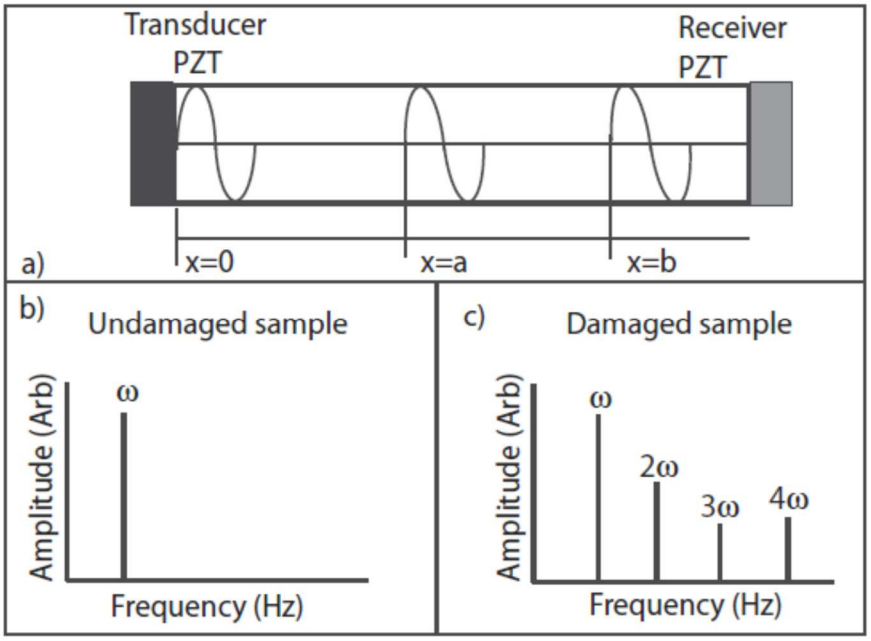

Figure 6 - a) Wave Propagation Schematic in Non-linear Medium b) Frequency Response in Undamaged Sample c) Frequency Response in Damaged Sample (Haller, 2007).

In general, there are three principal methods for ultrasonic measurement testing (NASA, 1999):

1) Pulse-Echo method: a piezoelectric element is placed on the tested material's surface and is supposed to receive and transmit ultrasonic waves. After applying the ultrasonic waves, they are reflected by the opposite side of the material or any layers, void spaces, and discontinuities. The reflected waves will be received by the same transducer and will be displayed by an oscilloscope. The thickness of the material and the location of flaws can be extracted in this method. Figure 7 shows the general schematic of this method.

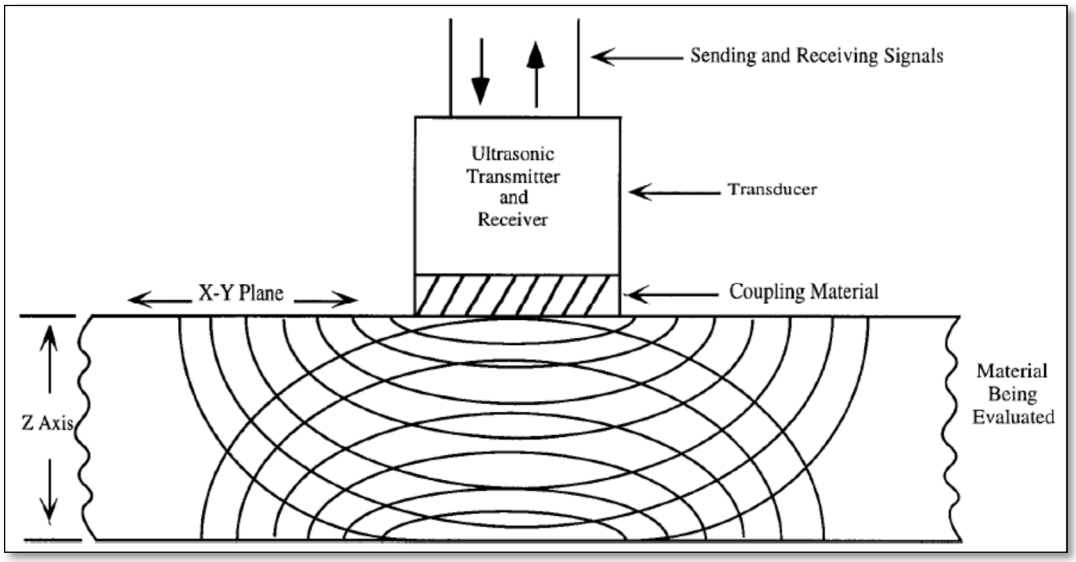

Figure 7 - Pulse-Echo Method of Ultrasonic Testing (NASA, 1999)

2) Through-Transmission method: there are two transducers used in this method, one is placed on one side as the transmitter, and the other is mounted at the opposite side as the receiver. The transducers should be installed in front of each other. This method is used for detecting the location of defects, inclusions, and flaws in multilayered and multicomponent materials. The general setup of this method is illustrated in Figure 8.

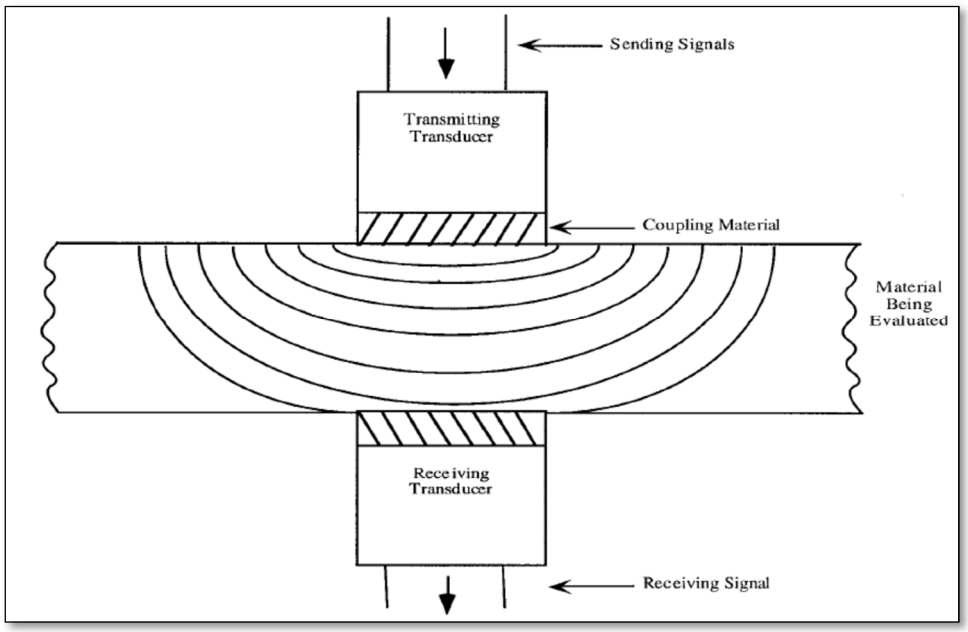

Figure 8 - Through-Transmission Method for Ultrasonic Testing (NASA, 1999)

3) Pitch-Catch method: In this method, an ultrasonic wave is sent at any angle to the material's surface, and the reflected wave is received at the reflected angle by the receiver. Detection the flaw's depth and location are possible with this method. Pitch-catch is used chiefly for cylindrical tubes and other non-linear parallel-sided surfaces (Figure 9) (NASA, 1999).

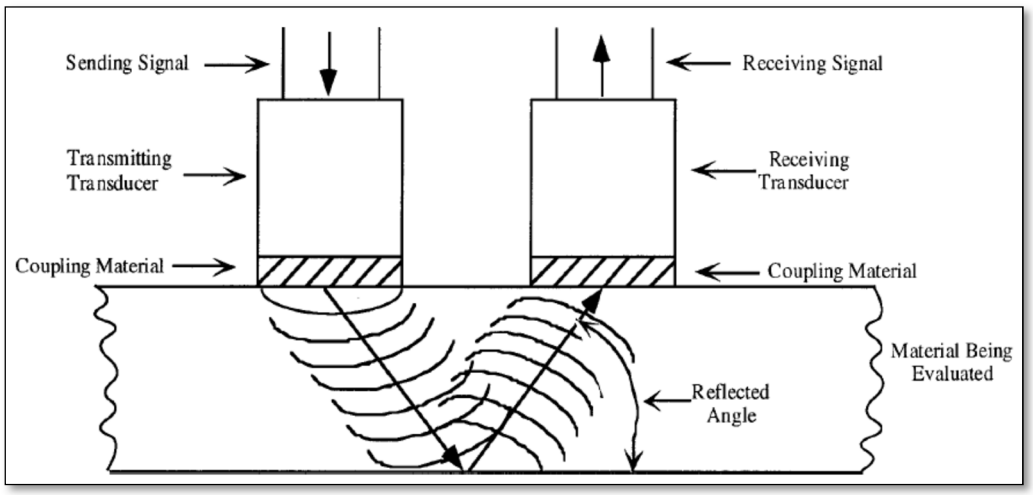

Figure 9 - Pitch-Catch Method for Ultrasonic Testing (NASA, 1999)

2.4.4 Wave Generation by Piezoelectric

The required device for generating and detecting the ultrasonic energy is called a transducer. A transducer is a device actuated by energy from one system to provide energy in any form to a second system. The most common conversion in ultrasonic is from electrical to ultrasonic energy in transmitters or ultrasonic to electrical energy receivers. Transducers can be electrical, mechanical, and pneumatic devices. Piezoelectric, electrostatic, magnetostrictive, and electromagnetic are electrical devices that convert electrical to ultrasonic energy or vice-versa. Among these electrical devices, piezoelectric and magnetostrictive devices are the most common to produce ultrasonic waves (Ensminger et al., 2012).

Discovered by the Curie brothers in 1880, piezoelectricity is also called "pressure electricity," which means a pressure applied along certain crystallographic axes produces electrical charges on the preferred crystallographic surface (Mason, 1950). The converse of the definition is also true. If voltage is applied between two preferred surfaces, stress or strain will be produced along axes of the crystal (Ensminger et al., 2012). Respectively, these are called the direct and inverse piezoelectric effects. Piezoelectric transducers are primarily used for ultrasonic measurement in solid materials, and due to high impedance mismatch, it is not efficient to use them in the air (Ultrasonic Nondestructive Evaluation Systems, 2015). A basic schematic of ultrasonic measurement by using transmitter and receiver is shown in Figure 10 (Ensminger et al., 2012).

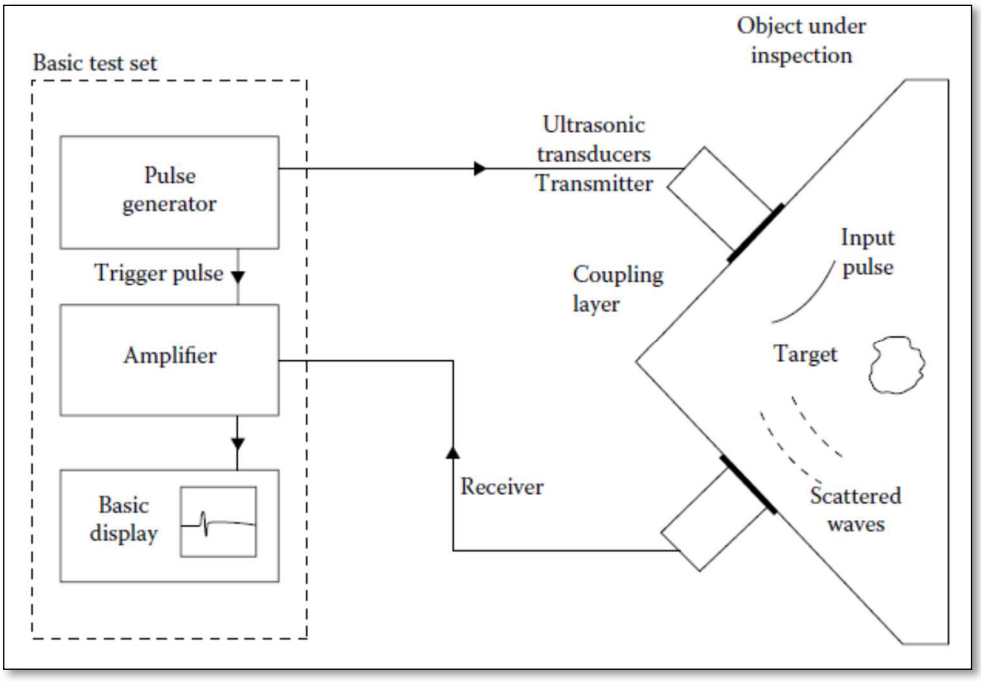

Figure 10 - A basic arrangement for ultrasonic measurement (Ensminger et al., 2012)

Simplification of wave generation and detection process helps better understand how the wave generation can be used for ultrasonic measurement. The process is that the transmitter generates the wave, and after passing through the material body, a receiver on the other side will receive it. However, the output trend is dependent on the sample's

structure and geometry, and as we see further, not just the first receiving wave but also reflections from the edges of the sample.

As displayed in Figure 11, if the path between the transmitter (T) and the receiver (R) is free of defects, the elapsed time/flight time, will be smooth. If the T- R space lacks structural homogeneity, the output signal will be dispersed, the elapsed time will be greater, and the velocity will be reduced. If the edge of a crack is closed to the T and R positions, the signal does not travel through a solid-air interface. Therefore, the signal path will be greater than the distance between two transducers, and the velocity will be lower than the sound characteristics in a normal structure. Finally, if a cavity existed between T and R inside the sample's structure and the wave hits the cavity, it will be largely reflected, and the time of flight will be hardly measurable (Ultrasonic Nondestructive Evaluation Systems, 2015).

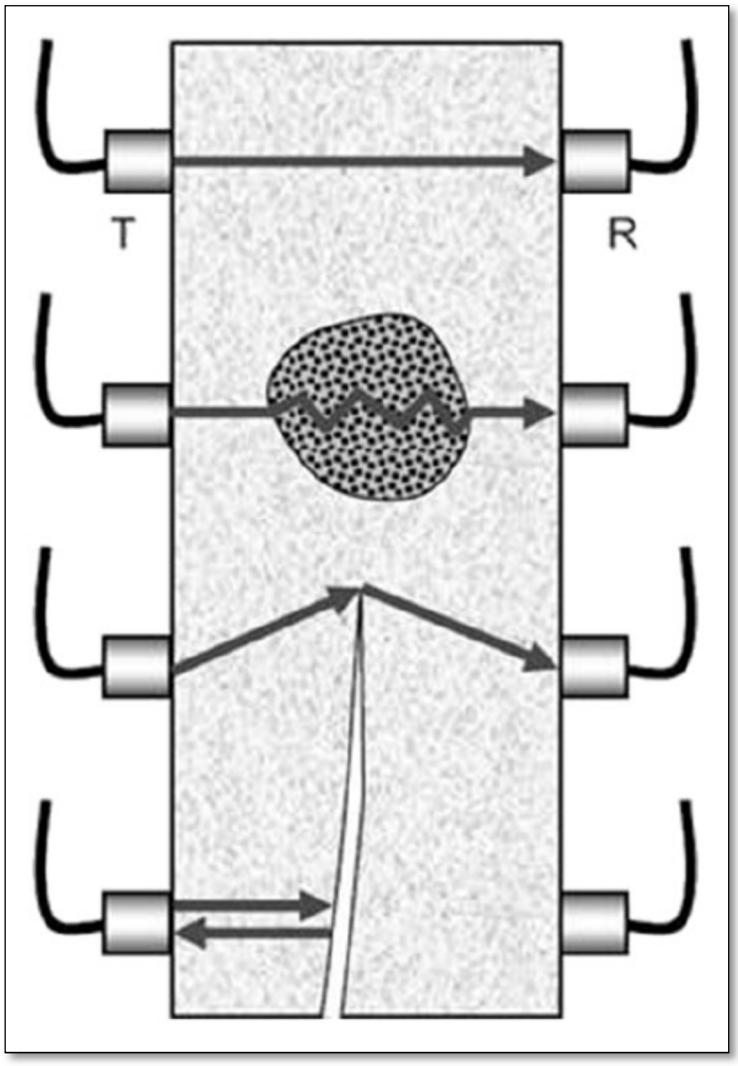

Figure 11 - Possible Paths to Receiver Signal (Ultrasonic Nondestructive Evaluation Systems, 2015)

2.5 Previous Studies

Reviewing what and how experiments have been done before helps to determine an efficient method for this thesis. This section provides the essential research works with the same concept and subject related to the thesis.

2.5.1 J.-K. Kim et al. – Compressive Strength Development of Concrete with Different Curing Time and Temperature

Published in 1998, the research team, including J.-K. Kim and his colleagues worked on the experimental investigation and developed a new concrete compressive strength model in various curing times with given temperatures. The curing temperatures used in this work were 5, 20, and 40 degrees Celsius while the compression tests were performed on the 1st, 2nd, 3rd, 7th, 14th, and 28th days. For this purpose, 324 concrete cylinder samples selected in two types in terms of water-to-cement ratio were prepared and subjected to the experiment. Water-to-cement ratios designed for the test were 0.55 and 0.35.

After performing the experiments, they concluded that samples in higher temperatures, 40°C, reached a greater strength value in the early days, although they showed a lower value at late days. However, at 5°C, samples attained a lower strength value in earlier days while almost the same strength value in later days as specimens subjected to 20°C. Moreover, the most important result of this study is that changing temperatures after three days of curing did not significantly affect compressive strength development (J.-K. Kim et al., 1998).

2.5.2 Rao et al. – An Ultrasonic Device for Nondestructive Testing of Oilwell Cements at Elevated Temperatures and Pressures

A research team from Haliburton Company published a paper regarding ultrasonic measurement, as a non-destructive test, of compressive strength of the cement at a high-pressure and high temperature well condition in 1982. The test design was based on transmitting the ultrasonic waves through cement slurry structure, converting the transit time to apparent compressive strength, and recording real-time data. Thirty-eight different cement compositions were used in cube geometry at this test with 5.08 cm (2 inches) length. For each designed mixture, tests were performed after curing times of 16 hours up to 90 days.

They observed a good correlation between transit time and compressive strength for cement H class at the first step. Then, they executed the test in the HPHT autoclave, which was modified to measure the ultrasonic wave's transit time while the cement was being cured under pressure and temperature. In this regard, they finally concluded that temperature and pressure could only cause small and predictable changes in the general correlation between transit time and compressive strength of the cement (Rao et al., 1984).

2.5.3 Shin SW et al. – Piezoelectric Sensor Based Nondestructive Active Monitoring of Strength Gain In Concrete

Shin SW and his colleagues performed a series of experiments to extend the applicability of Electro-Mechanical Impedance (EMI) sensing for monitoring and measuring the concrete's strength in 2008. EMI was sensed by Piezoelectric lead Zirconate Titanate (PZT) connected to the sample. In the EMI sensing technique, a piezoelectric-made transducer is bonded to the sample and used to indirectly measure the mechanical properties by receiving and reading the electrical impedance generated by the piezoelectric transducer. To execute the study, they divided the samples, with the same composition, into three different groups with different curing conditions; A) water bath curing, B) temperature and moisture controlled air curing with plastic sheet cover, and C) air curing without any temperature and moisture controlled. In total, forty-eight cylindrical samples were used (sixteen for each curing group). PZT dimension was 100 mm x 100 mm x 0.2 mm and attached to each cylinder after 24 hours of curing. They conducted the whole experiment by measuring the electrical impedance after 3, 5, 7, 14, and 28 days. The frequency range used in the experiment was 100 to 400 kHz.

In order to have more precise data and reduce the noise participation in the result, measurements were repeated ten times, and the average value for each set of samples was selected. The conclusion was that the compressive strength significantly increased up to 14 days, and afterward, the rate decreased for all three groups. The highest compressive strength was group A with 27.73 MPa on average, then group B and C, with 24.48 MPa and 19.25 MPa, respectively. In addition, they concluded that the EMI sensing technique is a really sensitive tool to monitor the compressive strength development and initial bonding between the PTZ transducer and the sample affects EMI reading values (Shin SW et al., 2008).

2.5.4 Wang et al. – Mechanical Characteristics of Cement-Based Grouting Material in High-Geothermal Tunnel

A series of experiments were performed to acquire the compressive strength of grouting materials under different temperatures and relative humidity by Wang and his colleagues. The purpose of the experiments was to discover the influence of environmental effects, including high temperature and relative humidity on mechanical properties of grouting materials in high-geothermal tunnels in China and study the failure characteristics. Ordinary Portland cement type 1 was used to prepare 70.7mm x 70.7mm x 70.7mm samples for sixty-fours. The specimens were cured and tested at different temperatures, including 20, 40, 60, and 80 degrees Celsius and relative humidity 25%, 55%, and 95%.

After performing the experiments, the stress-strain curve was obtained for the compressive strength tests shown in Figure 12. From point O to point A, the compression stress linearly increased with the strain. There was no change observed in the curve's slope at the OA segment. As the compression stress reached point A and continue increasing to point B, the slope grew nonlinearly, and the curve's slope became decreasing. The internal micro-cracks started expanding before reaching the peak (point B) with a slight cracking sound, but only a few micro-fracture appeared on the concrete's

surface. At the BC segment, where the stress-strain curve began to decline, the non-interconnected vertical cracks were created at the specimen's surface. The local structure inside the specimen had been damaged considering the rapid decline from point C to point D.

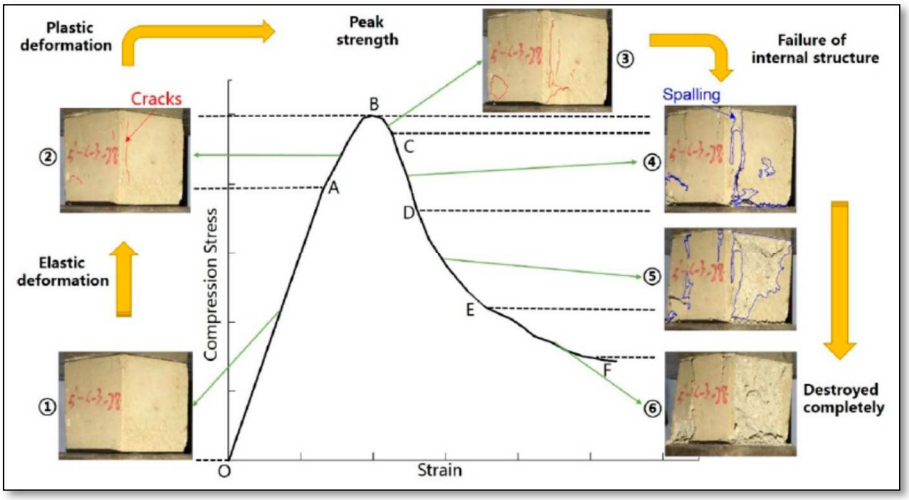

Figure 12 - Compression Failure Process (Wang et al., 2020)

Chapter 3 Experimental Apparatus

A general description regarding the equipment and apparatus used for executing the practical part of this thesis is explained in this chapter. All equipment listed below was provided by and located in the laboratory building of the petroleum engineering department of Montanuniversität.

3.1 Electronic Scale

Weight of required raw materials, including cement class G, water, barite, bentonite, and 3M glass additive, were measured using electronic scale FCB 3K0.1, manufactured by Kern (Figure 13). The weighing capacity and readability of the scale were 3.0 kg and 0.1 gr, respectively (Kern's official website). Refer to API RP 10B-2, the accuracy of the scale should be within ± 0.1% that the scale meets it.

Figure 13 - The Electronic Scale

3.2 Slurry Mixer

A mixer is a gear bottom-driven device used for cement slurry's preparation by mixing the ingredient of different compositions such as water, cement, and additives. Chandler engineering's constant speed mixer model 3260 (Figure 14) with a one-liter cup was used in this experiment. The built-in mixer program was set for the speed of 4,000 ± 200 and 12,000 ± 500 rpm according to API specification 10, while it was able to provide and manually set a constant mixing speed from 1,000 to 20,000 rpm (Chandler's Constant Speed Mixer Model 3260 Instruction Manual, 2018).

Figure 14 - Chandler Mixer Model 3260

3.3 Mud Balance

After preparing the cement slurry, its density should be measured and recorded. For this purpose, the Ofite atmospheric mud balance was used (Figure 15). The mud balance has four measurement units contains specific gravity (SP. GR.), pound per gallon (ppg), pound per cubic feet (pcf), and psi per 1,000 ft. Pound per gallon is considered as the primary unit in this thesis, while the samples' densities were recorded in SP. GR., as well.

Figure 15 - Ofite Atmospheric Mud Balance

3.4 Atmospheric Consistometer

Atmospheric consistometer model 1200 made by Chandler was used to determine the free-fluid volume (Figure 16). In general, the basic thickening time tests and slurry conditioning in atmospheric pressure conditions are measured by the atmospheric consistometer. It contains a stainless steel water bath that can be heated up to 93° Celsius. Two slurry containers with 28 cubic inches capacity are designed for pouring the slurry into (Chandler's Atmospheric Consistometer Model 1200 Instruction Manual, 2018). A motor rotates the slurry containers at 150 rpm based on API Spec 10A.

Figure 16 - Atmospheric Consistometer 1200

3.5 Ultrasonic Measurement Devices

3.5.1 Oscilloscope

An electronic instrument called oscilloscope is needed to display voltage signals as waveforms. In fact, an oscilloscope visualizes the voltage variation over time. PicoScope 3000 oscilloscope, shown in Figure 17, made by Pico Technology, was used for ultrasonic measurements visualization. It has four channels with 200 MHz analog bandwidth that

is able to generate 100,000 waveforms per second. Moreover, generating arbitrary waveforms is one of the main features of this instrument.

The associated software provided by Pico Technology for visualization of the oscilloscope's readings is PicoScope 6.

Figure 17 - Oscilloscope PicoScope 3000

3.5.2 Amplifier

A circuit that delivers more power to a load than is received from an input is called Amplifier (Glisson, 2014). An amplifier can amplify the input voltage, the input current, or both (Agarwal et al., 2005). It can be located at the first (input) stage to amplify the received current or voltage from a sensor, or at the last (output) stage to augment the delivered current or voltage to a load or can be placed as an interior circuit (Glisson, 2014). The amplifier PD200 from PiezoDrive Company was used (Figure 18). It was a high bandwidth and low noise amplifier with an output voltage range from 0 V to 200 V (PiezoDrive's P200 V7 Power Amplifier Manual and Specification, 2020).

Figure 18 - Power Amplifier PD200

3.5.3 Piezo Elements

Two piezoelectric elements, one as a receiver and the other as a transmitter, based on lead zirconate titanate (PZT) and barium titanate materials, were used for ultrasonic measurement at this project. The piezo element type was PIC255 and made by PI Ceramic GmbH company (Figure 19). PIC255 has a high Curie temperature, 350°C, and moderate permittivity (PI Ceramic GmbH, 2021). The critical temperature that particular material loses its permanent magnetic properties above is called Curie temperature

(Pasquale V, 2011). PIC255 is categorized as a "ferroelectrically soft piezo ceramic" type that can be easily polarized even at relatively low field strengths (PI Ceramic GmbH, 2021).

Figure 19 - PIC225 Piezo Element

3.6 Uniaxial Compressive Strength Equipment

The destructive test of the thesis was done by the uniaxial compression testing machine model "Quasar 200" from an Italian manufacturer, Galdabini (Figure 20). The maximum allowable load to apply on the specimen was 200kN. The accuracy of positioning reading was 0.002mm (2µm), and the movement speed of the top plate is selectable. The test result was shown as load-time and stress-strain plots in its associated software (Galdabini's Official Website, 2021).

Figure 20 - Galdabini Quasar 200 (Galdabini's Official Website, 2021)

Chapter 4 Methodology

In this chapter, each step of the conducted experiments is explained. It describes the calculations for specimen preparation, the preparation procedure, performing ultrasonic measurement as the non-destructive test, and executing the compressive strength test as the destructive one. Figure 21 shows the flowchart of the conducted experiments.

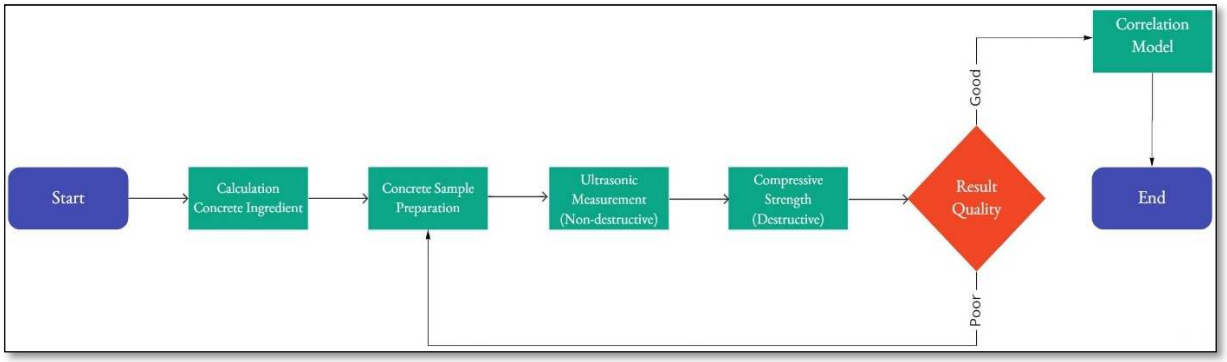

Figure 21 - The flowchart of the Executed Experiments

4.1 Cement Samples

4.1.1 Compositions Design

The weight of cement, water, and each additive were calculated based on API-RP 10B-2 (Equation 7). The department initially defined the density range, and the calculations were performed to meet the density's requirement.

$$\rho_{slurry} = \frac{M_{total}}{V_{total}} = \frac{(M_c + M_w + M_{add})}{(V_c + V_w + V_{add})}$$

(Equation 7)

Where ρ is the density of slurry calculated in [kg/m^3],

m is the mass of each ingredient [kg],

And V represents the volume of each component [m^3].

After calculation, conversion factor 1 ppg = 120 kg/m^3 was used to convert the density unit to a pound per gallon (Nelson et al., 2006).

Cement G class Grade High Sulfate-Resistant (HSR) was manufactured by Dyckerhoff GmbH Company according to standard ISO 10426-1/API Spec 10 A. Refer to Halliburton eRedbook's software, cement G density was considered 3.18, water 1.0, barite 4.23, bentonite 2.65, and 3M glass bubble 0.46 g/cc. All values were cross-checked with the technical data sheet provided by the manufacturers and confirmed.

High-grade barium sulfate, known as barite, was provided from Sirius E.S. and used as a weighting-up agent. More than 94% of mineral content was $BaSO_4$, and the moisture content was below 1% (Barite's Sirius E.S. Technical Data Sheet). Although barite is not commonly used in the industry, it is chosen due to its availability.

Same as barite, sodium bentonite was also supplied by Sirius E.S. company with 98-99% of bentonite and 1-2% of silica, crystalline, and cristobalite (Bentonite's Sirius E.S. Technical Data Sheet).

The latest additive used in this thesis was 3M Glass Bubbles HGS6000. The additive was manufactured and supplied by 3M Company and used as a lightweight agent. It was a chemically stable glass sphere made from soda-lime borosilicate. The additive was insoluble in water and can be used in deep water wells for improving cement performance by reducing density and viscosity. The composition can withstand wellbore pressures between 2,000 psi to 18,000 psi (JPT Staff, 2003). It contained 97-100% of glass and oxide and 0-3% silicon dioxide by weight (Glass Bubble's 3M Technical Data Sheet).

The following six cement compositions were designed and used in this thesis. Density ranges varied from 11.0 ppg to 16.0 ppg.

- Neat Cement (CN): Only class G cement mixed with water by 44% water-to-cement ratio.
- 3% Barite Cement (CBa3): 3% barite powder by weight of cement (BWOC) added to class G cement and water with 44% water-to-cement ratio added to the mixture.
- 6% Barite Cement (CBa6): 6% barite BWOC added to class G cement and water with 44% water-to-cement ratio added to the mixture.
- 0.8% Bentonite Cement (CBe08): Added 0.8% bentonite powder BWOC as an extender to class G cement and increased water-to-cement ratio to 54%.
- 2% Bentonite Cement (CBe2): Added 2% bentonite powder BWOC as an extender to class G cement and increased water-to-cement ratio to 70%.
- 19% 3M Glass Bubbles (C3M): Used 19% 3M Glass Bubbles powder BWOC besides 0.5% BWOC of bentonite with class G cement and added water to reach 73% water-to-cement ratio.

The following Table 2 shows the ingredient of each composition in detail. It should be noted that all measurements were done based on 600 cc total mixing volume as per API RP 10B-2 standard.

Cement Code	Cement Mass [gr]	Water Mass [gr]	Barite Mass [gr]	Bentonite Mass [gr]	3M Glass Bubble Mass [gr]	Measured Density [ppg]
CN	792.5	350.2	0	0	0	15.7
CBa3	789.3	347.3	23.68	0	0	15.9
CBa6	781	343.8	46.9	0	0	16.0
CBe08	696.8	375.8	0	5.6	0	14.8
CBe2	586	409.8	0	11.7	0	13.8
C3M	410.6	300	0	2.1	78.2	10.9

Table 2 - Cement Slurries Ingredients

To design the slurry recipe, the water-to-cement ratio was kept constant for CN, CBa3, and CBa6 compositions to minimize its possible effect on the ultrasonic measurement. Therefore, regardless of the barite BWOC, the water-to-cement ratio was kept at 44%, and the only parameter needed to vary was density and barite weight consequently.

As increasing bentonite proportion escalates the slurry's viscosity (Allan, 1999), we could not keep the water-to-cement ratio constant in both bentonite compositions (CBe08 and CBe2). An attempt was made to prepare a bentonite composition while keeping the 44% water/cement ratio. It was vain, since the slurry became very thick and was not naturally movable from the mixing cup. Therefore, the ratio was changed and increased to 54% and 70%, respectively, by increasing bentonite proportions to reach better the bentonite compositions' pumpability. Pumpability means the mobilization capacity of a slurry under pressure while its initial properties are maintained (Marc Jolin et al., 2009).

The C3M's slurry formulation was proposed by drilling chair of the university. The target density for this composition was the lowest value, 11.0 ppg.

4.1.2 Cement Preparation

The whole cement preparation process was done according to API recommended practice 10B-2. The electronic scale was calibrated in February 2021. At first, a dry and clean container's weight was measured and kept on the scale; then, the tare button was pushed in order to reset the scale's reading to zero. Hereafter, the required volume of freshwater with a temperature of 16°C was transferred to the container. The same procedure was applied for mixing the dry additives such as cement, bentonite, barite, and 3M glass bubble.

The preparation procedure for all six compositions is explained as follows:

1. Measuring the weight of water.
2. Adding the required water volume to the mixer's cup.
3. Measuring the weight of cement.
4. Measuring and adding the dry-powder additives to cement containers and manually mixing all compositions for two minutes.
5. Turning the slurry mixer on in automatic mode, the rotation speed was set to 4,000 ± 200 RPM in 15 seconds while adding cement and additives mixed before the one-liter cup.
6. Putting a lid on top of the cup and the built-in mixer program increases the rotational speed to 12,000 ± 500 RPM for 35 ± 1 seconds.
7. Stopping the mixer automatically after 50 seconds in total.
8. Removing the lid and starting pouring the mixed slurry into cubic and cylinder molds.

Before pouring the slurry into the mold and casting samples, the density of the mixed slurry was measured by the atmospheric mud balance. Before each density measurement, the accuracy of mud balance was checked by freshwater. The difference between calculated density using equation 7 and measured density was approximately 0.1 ppg. This could happen due to variation in water and chemical densities, measurement errors, and air trapped in the mixture (Ichim, 2017).

In order to ease the removal of the sample from the cylinder and cubic molds, a thin layer of inert and non-corrosive industrial grease was applied to the mold's walls. Furthermore, it was beneficial for better sealing of molds and better screw lubrication. The slurry was poured into the molds at half of the mold's height and then was stirred by a puddling rod to remove air bubbles from the slurry. Each sample was stirred approximately 30 times. There was no top plate over molds used in this thesis.

In terms of temperature and pressure, the curing condition was atmospheric. During sample preparation and hardening, the average room temperature was 23° C. Topside of the samples was constantly in contact with air. After one day, the samples were removed from the molds and kept in the same temperature and pressure conditions.

4.1.3 Sample Geometry and Quantity

Two different geometries were used in this thesis: cubic and cylindrical.

Cube sample dimension was based on API RP 10B-2, 2″ x 2″ x 2″ (50.8 mm x 50.8 mm x 50.8 mm). After removing samples from the molds, all three dimensions were measured and recorded as they were necessary for ultrasonic measurement as well as compressive strength tests. Although the length measurements did not have a considerable difference with initial cube molds, the average of three dimensions was considered for compressive strength calculation, while for ultrasonic, only the length between two sensors was taken into account.

Same as the cube samples, the internal diameter and length of cylindrical samples were measured as well. The cylinder mold was made from polypropylene material. In accordance to Eurocode 7 standard, the height-to-diameter ratio in cylindrical samples should be between two and three (Marques et al., 2015). Therefore, as the pipe's ID was 28mm, then the samples were prepared at the height of 56mm. Height measurement was performed from two sides, and the average of two measurements was considered the final length for the ultrasonic test.

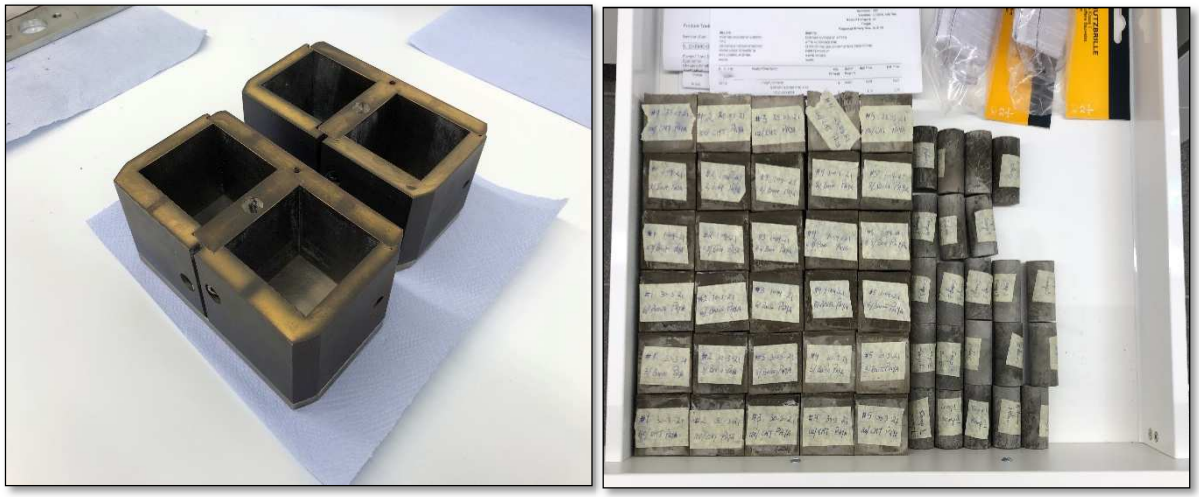

Figure 22 - left) Cube Molds right) Prepared Cubic and Cylindrical Samples

In total, more than a hundred samples in both cubic and cylindrical shapes were prepared for the project. The exact number for each ultrasonic and compressive strength test are listed in the following Table 3.

Cement Code	Geometry	UCS Test	Ultrasonic Test	Total Number
CN	Cube	15	5	20
	Cylinder	5	5	
CBa3	Cube	17	5	22
	Cylinder	5	5	
CBa6	Cube	14	5	19
	Cylinder	5	5	
CBe08	Cube	17	5	20
	Cylinder	3	3	
CBe2	Cube	17	5	21
	Cylinder	4	4	
C3M	Cube	15	5	15
	Cylinder	0	0	

Table 3 - Cement Sample Quantity

4.1.4 Free-Fluid Test

Another test performed on all slurries was the free-fluid test (formerly free water test). "*A layer of nonparticle-laden fluid on top of cement slurry*" is called free water (Nelson et al., 2006). A continuous water phase formed on top of the slurry shows that a certain amount of water is dropped out of the slurry. The free water volume should be calculated per unit volume of slurry. This volume indicates the stability of cement slurry settlement. Unequal density distribution and inconsistent strength of set cement can be consequences of excessive free-fluid in the slurry (Wan Renpu, 2011).

As per API Spec 10A, the free fluid for class G cement shall not exceed 5.9% while in actual field applications, specially for cementing complicated wells such as high deviated, horizontal, or high pressure high temperature wells, the free fluid value should be particularly zero. The used formula for calculating the free-fluid percentage is shown in (Equation 8):

$$\varphi = \frac{V_{FF} * \rho}{m_s} * 100$$

(Equation 8)

Where φ represents free-fluid in the slurry in percentage,

V_{FF} shows the volume of the collected free-fluid [milliliters],

ρ is the slurry's specific gravity [S.G.],

and m_s shows the initial recorded mass of the slurry [gr].

The procedure of performing the free-fluid test is described as below:

1. Filling slurry containers belong to the atmospheric consistometer (Refer to section 3.4).
2. Assembling all associated parts with the containers and placing them inside the consistometer in less than a minute.
3. Starting stirring the slurry by turning the consistometer on at temperature 27°C ± 2°C and atmospheric pressure for 20 minutes ± 30 seconds.
4. Transferring the slurry from the containers into a 500 milliliter conical flask in less than one minute.
5. Recording the actual mass transferred.
6. Keeping the flask in a vibration-free table with atmospheric pressure and room temperature 23°C ± 3°C for two hours ± five minutes.
7. After the mentioned period, removing the fluid, which has been developed on top of the slurry, by a syringe or pipette with an accuracy of ± 0.1 milliliters.
8. Recording the milliliter free-fluid and converting it to percentage using equation 8.

The free-fluid test was performed for all prepared slurries with different densities, and the result is illustrated in Table 4.

Cement Code	Density in ppg [S.G.]	Free-fluid [%]
CN	15.7 [1.88]	3.81
CBa3	15.9 [1.91]	3.87
CBa6	16.0 [1.92]	2.95
CBe08	14.8 [1.78]	3.31
CBe2	13.8 [1.66]	4.92
C3M	10.9 [1.31]	0.96

Table 4 - Free-fluid Test Result

4.2 Ultrasonic Waves Measurement

4.2.1 Experiment Setup

Earlier studies have shown that surface roughness influences the mean amplitude of the received signal (Wang et al., 2018) and greatly degrades signal-to-noise ratio (Nagy et al., 1993). The ratio compares the defect signal to other background reflections, categorized as noise (Chiou et al., 2016). Therefore, both surfaces of the samples were polished by a paper file. A smooth surface helps to reduce noises and errors in ultrasonic measurement and increase adhesion between piezo elements and the sample.

The experiment was executed for each sample individually in two ways; air-coupling and gel-coupling. In an air-coupling way, the transducers were connected to the material's body without applying the gel layer. There are two main problems for using air as coupling between the sample and transducer:

- A considerable difference between of acoustic impedance between the air and a solid
- High absorption of ultrasonic waves in case of propagating in the air

The mentioned problems cause the transferred energy by transducers to become very low (Perez, 2008). In other words, most of the power is reflected, and a small amount is transmitted into the sample via air-coupling way.

On the other hand, the gel-coupling is when a gel layer is applied to the contact point between the piezo element and the sample. The advantages of using a gel-coupling for ultrasonic measurements are:

- It transfers higher energy level in and out of the sample
- It makes a better attachment and connection between the transducer and the material (Ladislav Carbol et al., 2015).

In order to minimize errors during measurement and stabilize the piezo elements at the designed spots on the sample surface, a screw clamp was used and placed on the piezo elements. The screw was tightened for the element's fixation.

Two piezoelectric PIC255 transducers, one as transmitter and the other as a receiver, were attached to both sides of the sample, parallel and at the same line position to measure travel time. The positions of the transducers and the schematic of the ultrasonic measurement setup are depicted in Figure 23.

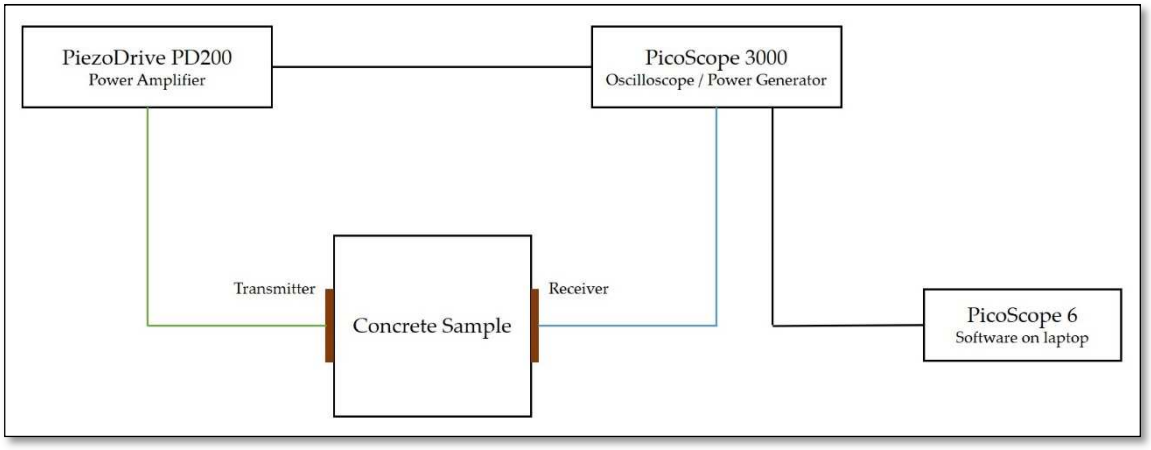

Figure 23 – Schematic Ultrasonic Measurement Setup

Power generator PicoScope 3000 generates a 4V electrical power transferred to the amplifier, PiezoDrive PD200, via cable. Then, the amplifier augments twenty times the received signal. Therefore, an 80V signal is delivered to the transmitter by the cable (green). For all cement compositions and ultrasonic measurements, the frequency was set at 400 kHz. The piezoelectric transmitter element changes the electrical power to ultrasonic form and sends it into the specimen. The velocity of the ultrasonic wave, formed by the piezoelectric, is dependent on the cement specimen property. One of the leading cement properties, as discussed earlier, is compressive strength. Compressive strength increases over time (Iffat, 2016). After passing the length of the specimen, the ultrasonic wave hits the opposite side of the specimen on which the receiver piezo element is installed. This hitting causes a sharp peak in the receiving voltage.

Contrary to what happened in the transmitter element, the ultrasonic wave is transformed into an electrical form by the receiver element. Thereupon, the electrical energy is delivered to the oscilloscope PicoScope 3000, which is connected to the receiver piezo elements through another cable (blue). The oscilloscope shows the voltage amplitude variations, and calculating the transit time will be possible afterward. Figure 24 shows the setup.

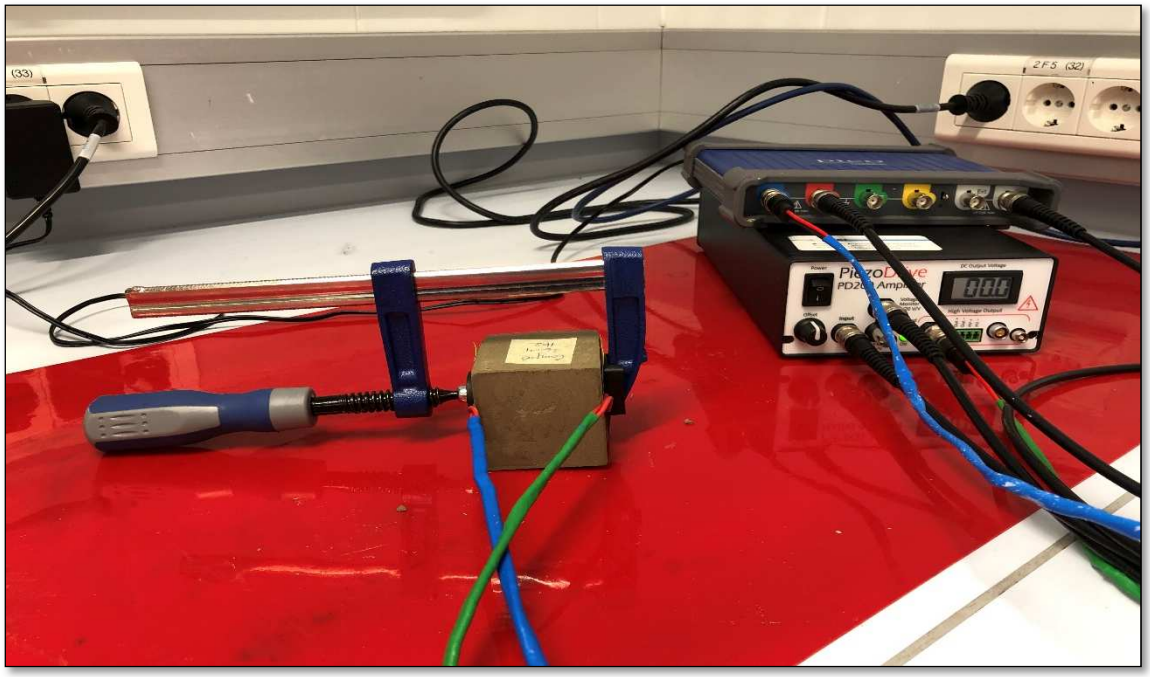

Figure 24 - Ultrasonic Measurement Setup During Experiment

4.2.2 Transit Time and Wave Velocity Measurement

In Figure 25, the red curve shows the transmitted voltage by the transmitter, and the blue curve represents the received voltage. The time at each peak is displayed by selecting the peak.

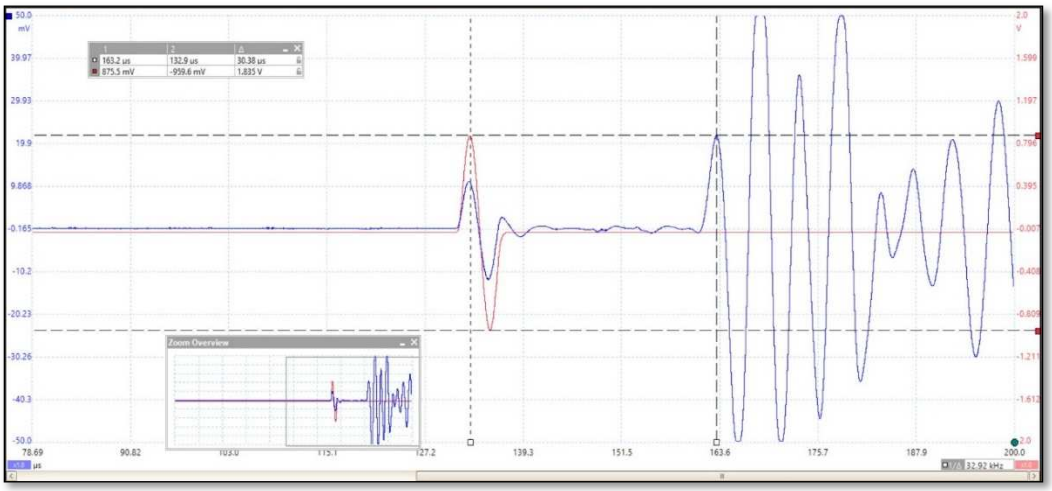

Figure 25 - Transmitter and Receiver Curves

The final step of the ultrasonic measurement is calculating the wave velocity based on the oscilloscope's given chart. (Equation 9) is used in this thesis for this purpose:

$$V = \frac{Path\ Length}{Transit\ Time} * 1000$$

(Equation 9)

Where V is the wave velocity [m/s],

Transit time is the period of time that the wave travels from the transmitter to the receiver [microsecond],

And the path length is the distance between the transmitter and the receiver elements [mm] (Estévez et al., 2020).

4.3 Compressive Strength Measurement

A uniaxial compressive strength test, UCS, was performed by placing the cement plug samples (2) between the fixed plate (3) and the moving carrier (1) shown Figure 26 - left.

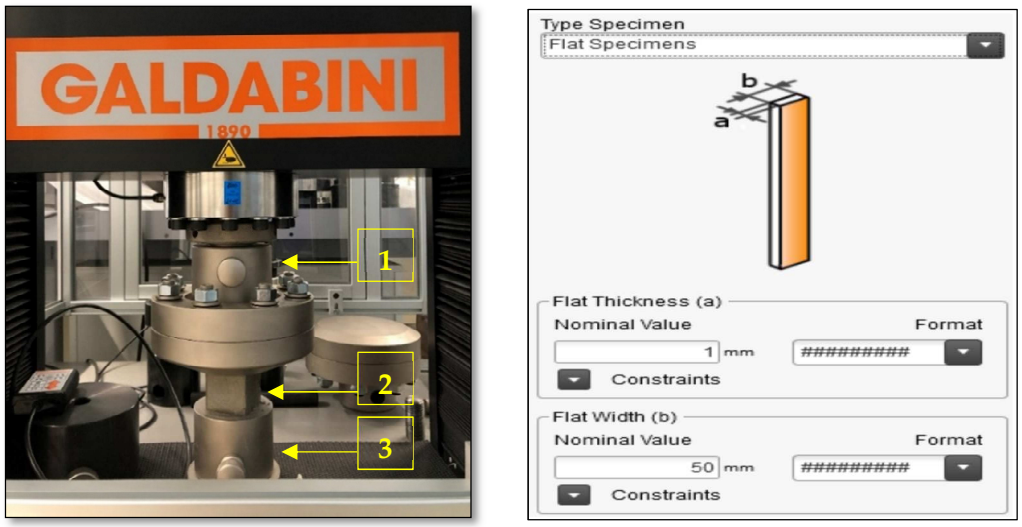

Figure 26 - left) The UCS Setup right) Flat Sample Setting

The experiment for each sample was done in "axial displacement controlled" mode. At this mode, the displacement rate of the moving carrier is kept automatically constant by the device's PLC. The axial displacement-controlled mode can prevent unstable and rapid failure of the cement sample (K.-H. Schwalbe et al., 2007). In the other hand, the cement under another method called “load controlled” will fail destructively which can have a big impact on the results (R.P.L. Nijssen et al., 2010).

For performing the UCS test, it was first to select the appropriate sample geometry in the associated software. The chosen geometry was the flat type. As shown in Figure 26 - right, two dimensions had to be entered into the software. In accordance to ASTM D2166-06, the displacement rate should be between 0.5%/min to 2%/min of the sample’s initial height. Therefore, the axial displacement rate was set at 1millimeter/minute which is equal to 2%/minute of the initial height.

After starting the test, the rest of the steps were done automatically. The moving carrier came down at the controlled speed and was applying load on the surface of the sample

until it failed. Meanwhile, the load-time (Figure 27) and stress-strain charts were being plotted on the screen. A group of data, including deformation, testing time, strain, friction, Poisson ratio, elongation, and energy, and compressive strength were extracted from the software as an output excel file for each sample.

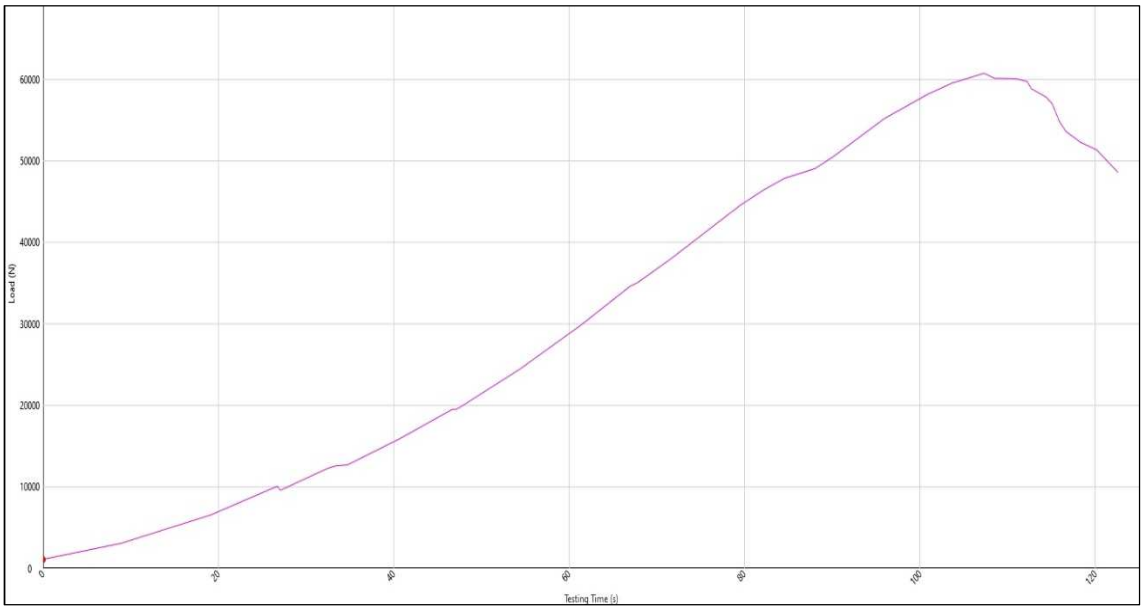

Figure 27 - A Load-Time Chart from the UCS Unit

4.4 Data Acquisition

The compressive strength, ultrasonic wave velocity, aging, and density are the leading group of data in this thesis. However, aging and density ranges are defined prior to starting the experiments. They can be categorized as "primary data," but the compressive strength and wave velocity are measured and calculated after performing the experiments. As they are the result of the experiments, hence they can be called "secondary data."

The primary data are single and absolute, while the secondary data are not absolute. In fact, the average value of compressive strength and ultrasonic wave velocity was considered as the final value in specific aging time for each composition. The value, which had a difference more or less than ten percent of the average, was excluded from the result.

The second group of data is including the additive-to-cement ratio (barite and bentonite), water-to-cement ratio, and free-fluid percent. Data such as additive- and water-to-cement ratios are designed at the initial steps of the experiment, and free-fluid percent works as the API standard's validator. In other words, these data are required for designing and making the cement samples for the experiment execution. Consequently, any change in these data can lead to variation in the primary data and the final result.

Chapter 5 Result and Discussion

The result of the performed experiments associated with their analyses is provided in this chapter. The findings are classified into two groups:

1. Numerical values, including the numbers and values which have been achieved by performing the experiments,
2. Analytical values, including the parameters and substances that can affect the numerical values.

In this chapter, first, the experiment is explained generally, then the ultrasonic wave velocity measured by air-coupling and gel-coupling are reviewed. Afterward, the compressive strength values are shown; after that, the correlation between the compressive strength and ultrasonic wave velocity is discussed.

5.1 The Experiment in General

The experiment consisted of three phases:

- Sample preparation phase
- Non-destructive phase (ultrasonic wave velocity measurement)
- Destructive phase (uniaxial compressive strength measurement)

The density range of the samples varied from 10.9 ppg up to 16.0 ppg. To do so, different additives were used. Barite was used as weighting agent with two different percentages, bentonite was selected as an extender to reduce the density in two different percentages, and the 3M glass bubble was also used to decrease the density and be compared with bentonite. Plus, the neat cement G was selected as the baseline composition. The exact number of 117 cement samples in six different compositions with different cement, additive, and water ratios was defined, designed, and made in this thesis.

Moreover, cylinder and cube shapes were selected to be compared together. For C3M composition, cylinder sample preparation was not successful as they were too weak and fragile, and during sample removal from the molds, all samples got destroyed. For the rest of the compositions, both cube and cylinders were available and measured for ultrasonic wave velocity. However, the cylinder samples were tested only one day, which did not give a valuable and broad range of data. Hence, the compressive strength result of the cylindrical samples was not mentioned in this thesis. The quantity and geometry of tested samples for both ultrasonic and compressive strength tests are shown in Table 3.

Right after slurry preparation, the free-fluid test was performed and the results met the API standard's requirement. Check Table 4.

The ultrasonic wave velocity and compressive strength measurements were done in five aging times, including the first, third, seventh, fourteenth, and twenty-first day. On each day, cubic and cylinder samples were tested, and data were recorded.

Five cubic and five cylindrical samples in CN, CBa3, and CBa6 compositions were selected for the ultrasonic wave velocity test, and they were all tested in different aging days. However, for CBe08 and CBe2, as the samples were destroyed during removal

from the cylinder molds, three and four samples were tested for the wave velocity measurement.

Furthermore, five samples in cylindrical and cubical geometries (total ten) for the whole six cement compositions were tested for compressive strength in all aging days.

5.2 Observations and Data Interpretations

5.2.1 Air-coupling Vs. Gel-coupling for Ultrasonic Measurement

One of the thesis's purposes was comparing the difference between the ultrasonic wave velocities measured with and without applying a thin layer of gel, which means air-coupling. For this purpose, all samples were tested with air-coupling at the first step, and immediately after performing the test, a thin layer of gel was applied between the oil well cement sample and both transmitter and receiver sensors. The test was redone to gain both values and compare them together.

Neat Cement

In cubic samples, the difference in measurement with and without gel decreased by time. On the first day of measurement, the difference was 1.26%, while it changed to 0.43% on day fourteenth. At these measurements, the wave velocity measured with gel-coupling was always higher than the ones with air-coupling. However, on day twenty-one, the gel-coupling velocity was less than air-coupling with 0.57%. The reason for this change in trend was because of changing the piezoelement sensor due to some functional problems.

The rate of decrease in cylindrical samples was not similar to the cubic samples. In fact, the decreasing rate was not linear. For example, the gel-coupling measurement was 1.35% higher than air-coupling on the first day, while the difference increased to 2.10% on the third day, followed by decreasing to 0.78% on the seventh day. As cylindrical samples' top and bottom surfaces were polished by hand, this change can be due to surface roughness. Total ultrasonic wave velocity was decreased in both gel- and air-coupling measurements. As explained earlier, it happened due to changing the transmitter sensor as it was not functioning.

In general, the total average difference between gel-coupling and air-coupling in the whole five aging days was 0.45% and 0.85% for cubic and cylindrical samples, respectively. The positive value shows the gel-coupling velocity is higher than the air-coupling. This difference is illustrated in Chart 1.

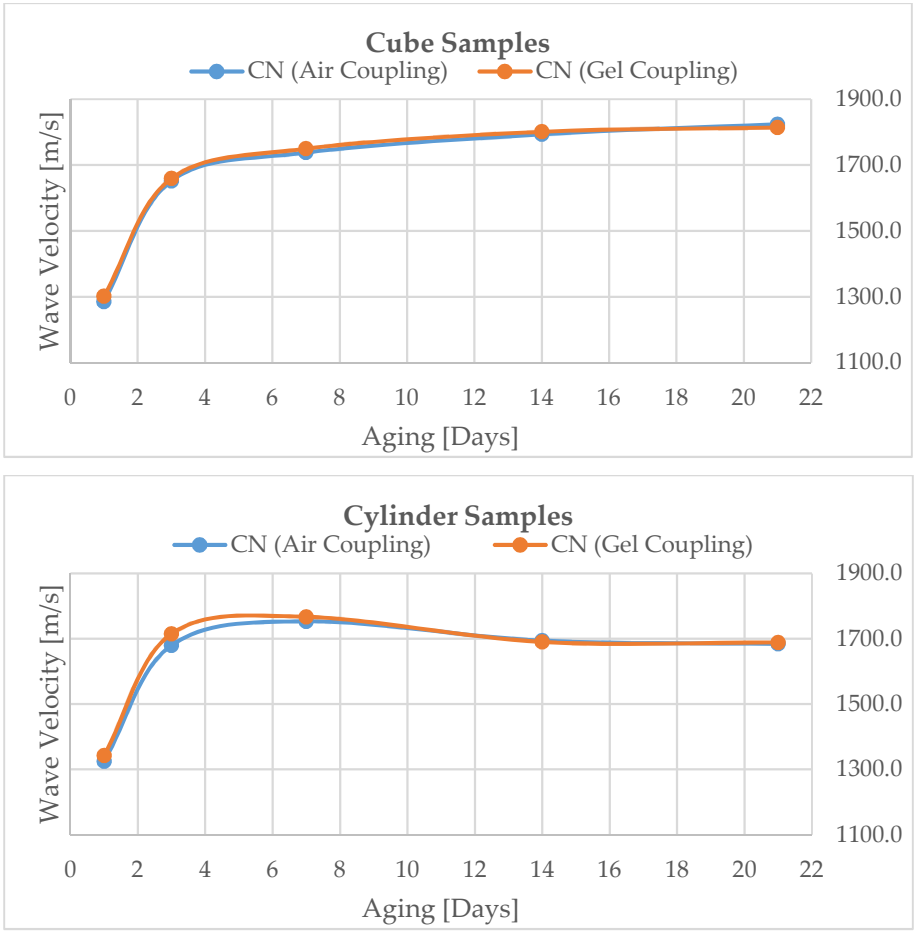

Chart 1 - CN Ultrasonic Wave Velocity: top) Cube Samples bottom) Cylinder Samples

Barite Cement

Similar to the neat cement, the difference in measurement for both three and six percent barite cements (CBa3 and CBa6) decreased over time. On the first day in both compositions in cubic shapes, the differences were 1.19% and 1.70%, and these values decreased to 0.19% and -0.3%, respectively. Here, the negative value means the air-coupling was higher than gel-coupling, which can be a measurement error.

Although the decreasing rate was observed for the cylindrical samples, its value was higher than that of cubic samples on the same day. The reason can be due to the surface roughness in a cylindrical mold. Chart 2 shows that the ultrasonic velocity became lower on the fourteenth and twenty-first day compared to the seventh day in cylindrical geometry, while in cubic molds, the ultrasonic velocity was always increasing. Changing the transmitter sensor due to its malfunction is why the measurement error in cylindrical samples after the seventh day.

In summary, in both cubes and cylinders and three and six percent barite compositions, the average difference in wave velocity with and without gel decreased over time. For CBa3 in cubic molds, the average wave velocity difference was 0.60%, while for CBa6 was 0.71%. In cylinder molds, the average for CBa3 and CBa6 were respectively 2.34% and 1.36%.

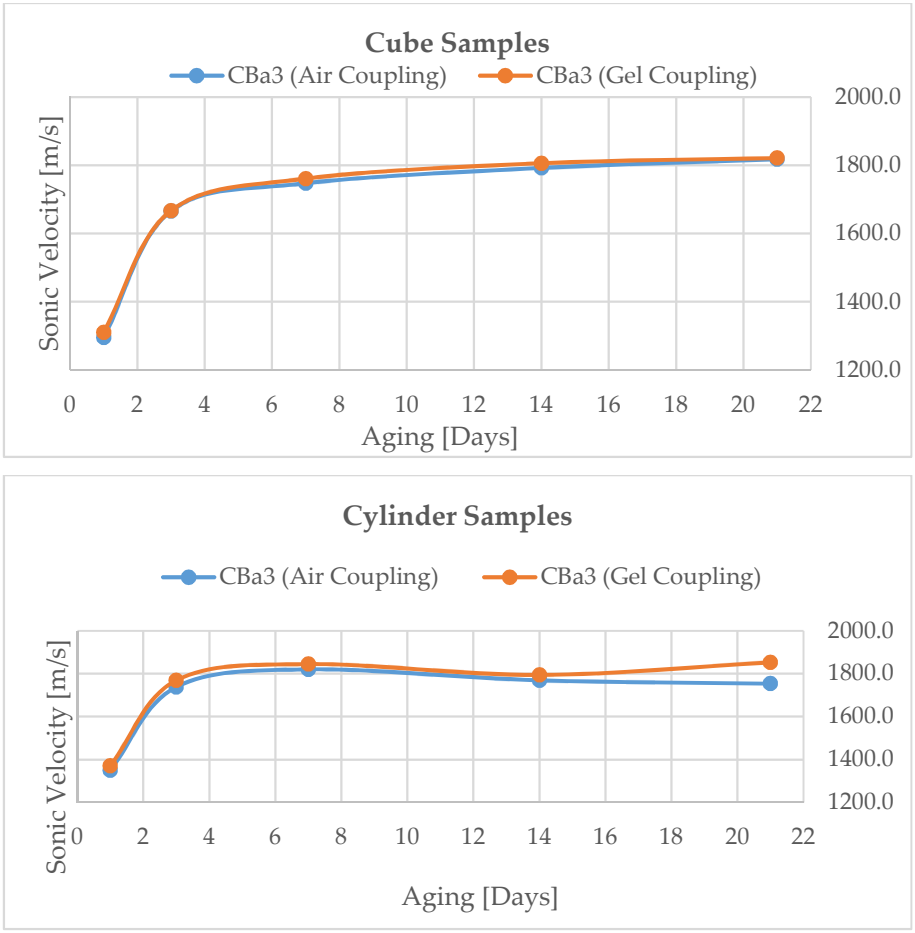

Chart 2 - CBa3 Ultrasonic Wave Velocity: top) Cube Samples bottom) Cylinder Samples

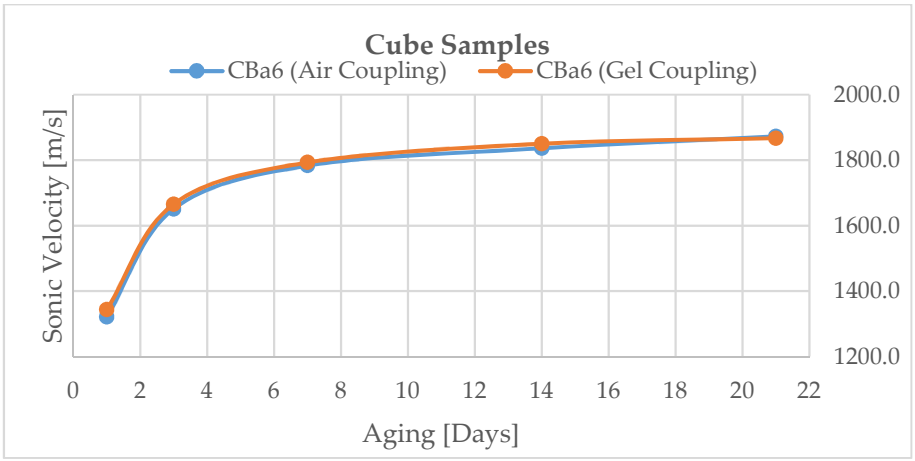

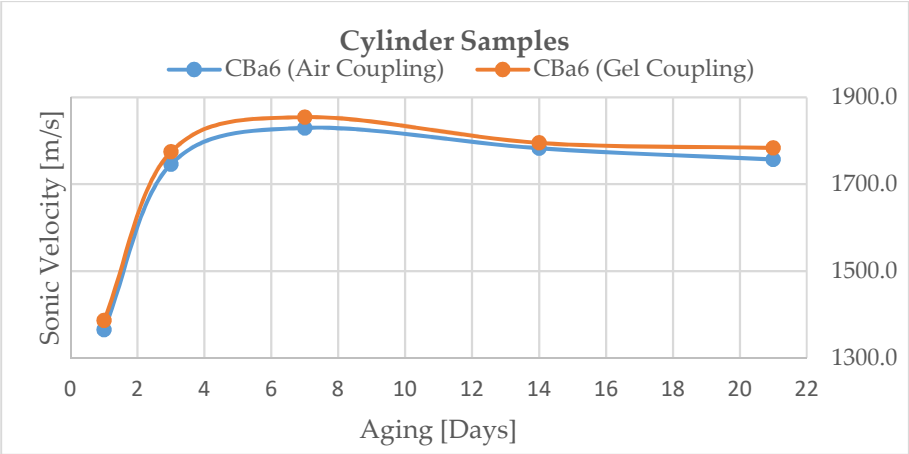

Chart 3 - CBa6 Ultrasonic Wave Velocity: top) Cube Samples bottom) Cylinder Samples

Bentonite Cement

The difference between gel-coupling and air-coupling ultrasonic wave velocity measurements decreased in bentonite cement in cubic and cylindrical shapes by passing the time, regardless of bentonite-to-cement ratio. On the first day, in cubic shape, the difference was 2.05% for CBe08 and 1.88% for CBe2 and then decreased to 0.39% and 0.70%, respectively. The almost same thing occurred in a cylindrical shape.

Similar to CN, CBa3, and CBa6 measurements, after day seventh, the velocity value decreased due to replacing the transmitter sensor as it was not working. The error probably occurred because of the samples having a high surface roughness. Similar to previous cases. On day twenty-first, the difference in measurement was negative in cylindrical samples, which means the air-coupling value became higher than the gel-coupling by 1.23% that could be owing to practical difficulties of the gel application and prob-surface contact.

To sum up, the average difference in wave velocity for bentonite cement with 0.8% and 2% bentonite-to-cement ratios in cubic shape were 0.79% and 0.89%, and in a cylindrical shape, they were 1.36% and 1.09%.

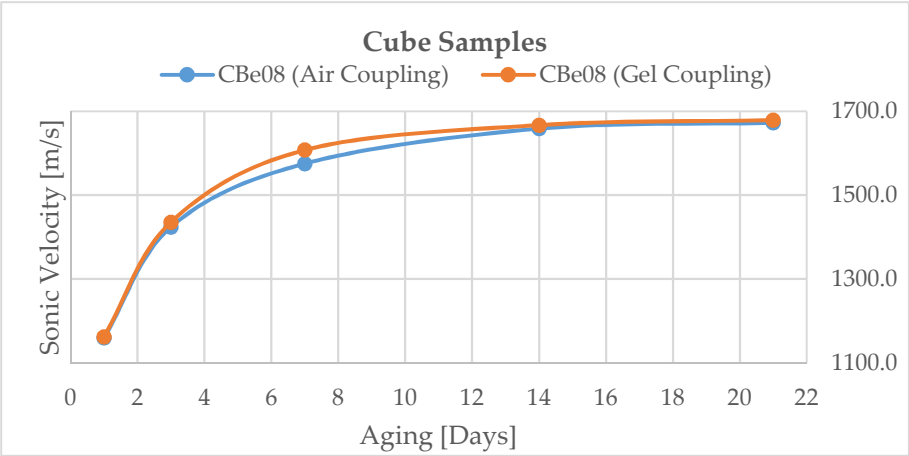

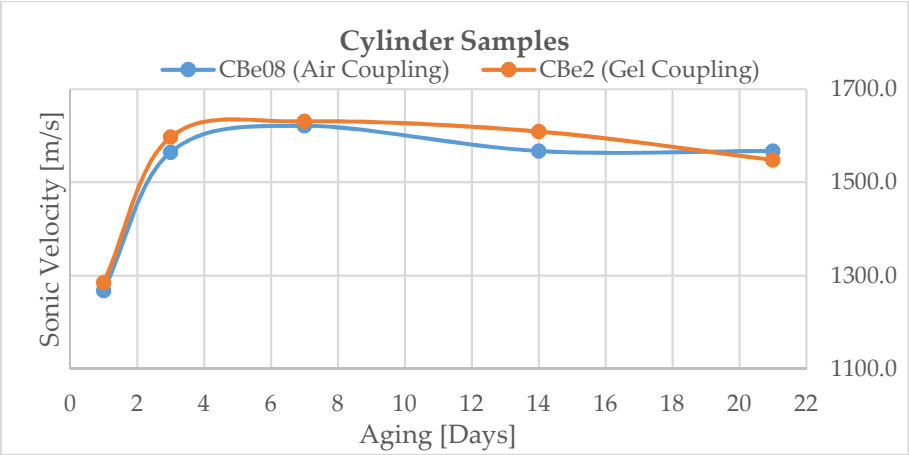

Chart 4 - CBe08 Ultrasonic Wave Velocity: top) Cube Samples bottom) Cylinder Samples

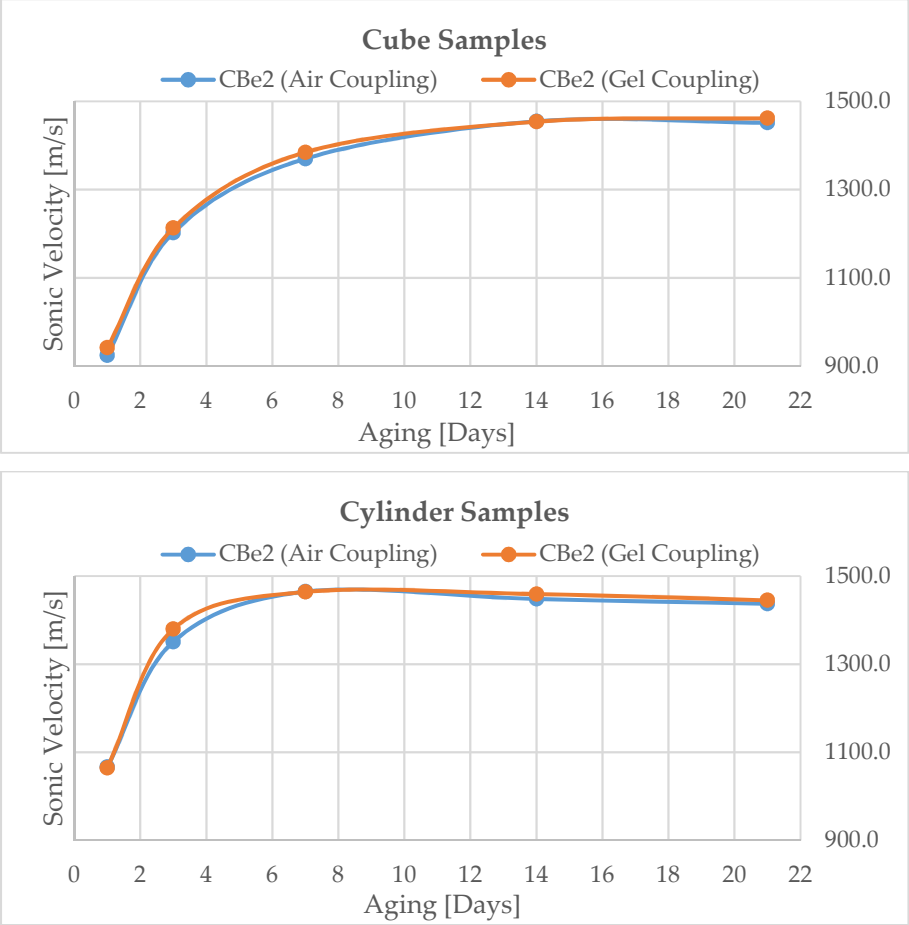

Chart 5 - CBe2 Ultrasonic Wave Velocity: top) Cube Samples bottom) Cylinder Samples

Enhanced Lightweight Slurry (3M Glass)

Chart 6 shows the slight difference between the gel-coupling and air-coupling measurements for ultrasonic wave velocity in the C3M composition in cubic molds. The difference decreased by passing the time, same as other compositions. The decreasing rate was relatively constant on the first day of measurement, the difference was 0.8%,

and the average of all five days of difference measurement was also 0.8%. In all measurements, the gel-coupling measured value was higher than the air-coupling value.

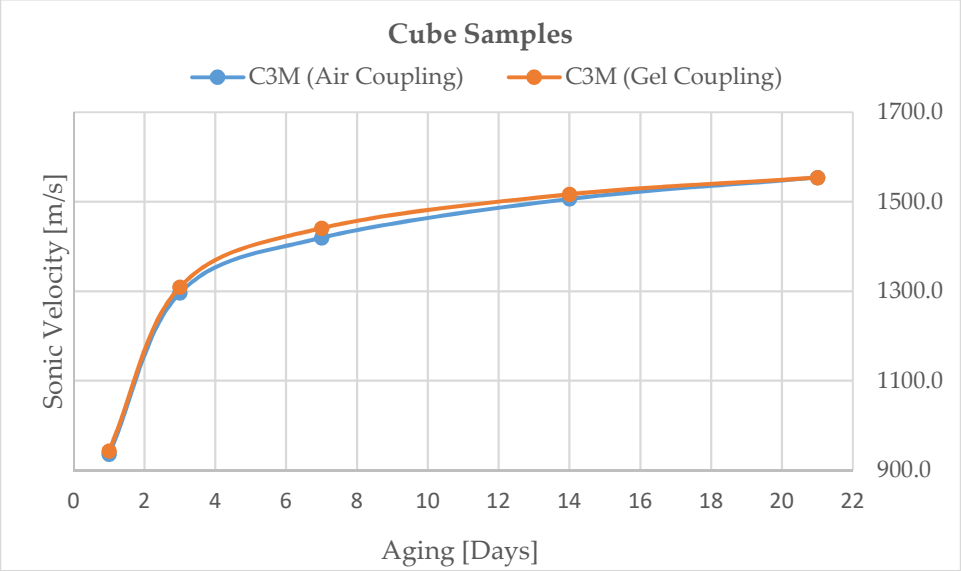

Chart 6 – C3M Ultrasonic Wave Velocity in Cube Samples

5.2.2 Ultrasonic Wave Velocity Development

The effect of each additive in all compositions on the propagation speed of ultrasonic waves was another objective in this thesis. In this regard, all cubic and cylindrical samples were examined in the same environmental situations at the same aging days with the specific device for ultrasonic wave velocity. It should be noted that the gel-coupling results were considered for this section.

• Role of Barite

The first three compositions, CN, CBa3, and CBa6, were designed to check the role of barite in ultrasonic wave velocity development. The idea to keep the water-to-cement ratio constant at 44% has come from this viewpoint. Making different compositions with barite-to-cement ratio besides using the neat cement, which had only water and cement, made this comparison possible, and the role of barite can be checked and studied. Considering that the CN had no barite, it was chosen as the baseline composition to check the role of barite.

A general trend of increasing the wave velocities of all compositions with cubic geometry is shown in Chart 7. The difference between wave velocity in the neat cement and 3% barite cement was almost close to zero in cubic samples. The maximum difference was 0.71% that happened on the first aging day, and the minimum was 0.28% on the fourteenth day. The average difference between the CN and CBa3 compositions was 0.51%.

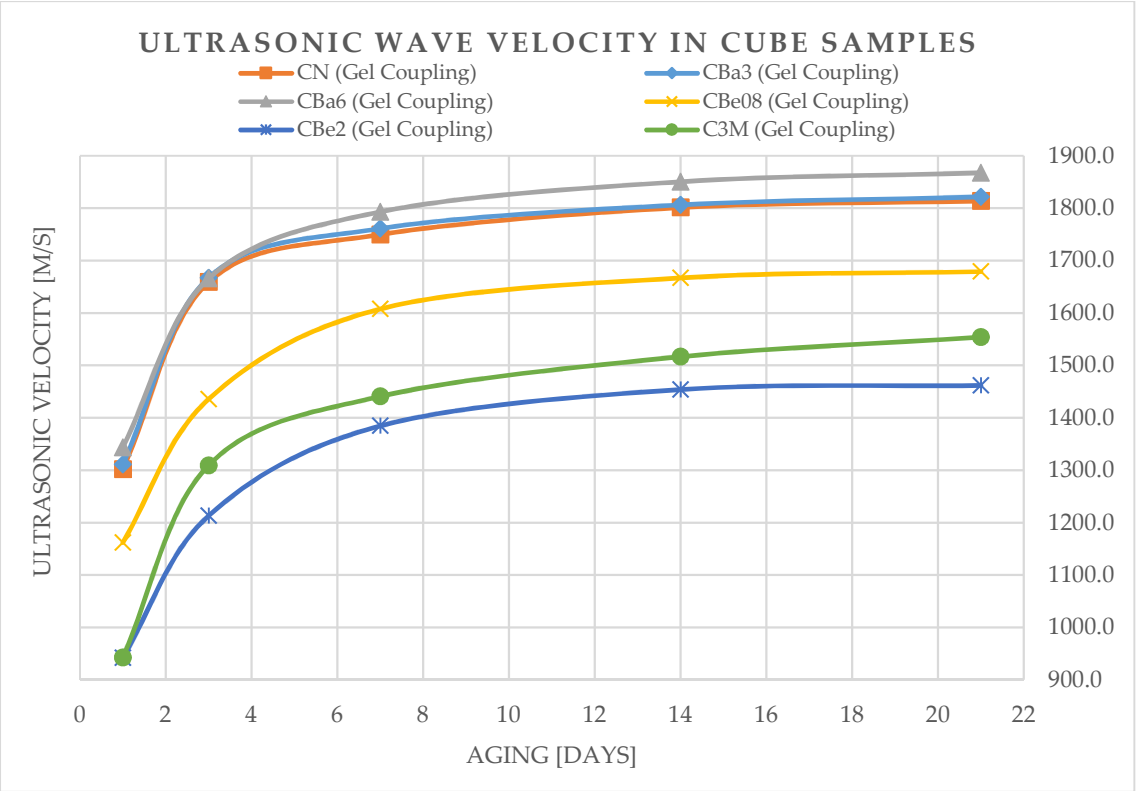

Chart 7 - Ultrasonic Wave Velocity in Cube Samples

While the difference between the CBa3 and CBa6 compositions was considerable. On the first day of measurement, the difference was 2.5%, and later it was never less than 1% between these two compositions. The difference rate was almost the same in each specific aging day, leading the difference average in ultrasonic wave velocity to 1.84%.

Comparing the CBa6 and CN compositions showed a similar result to the CBa6 and CBa3. The first-day difference was 3.22%, and then it slightly decreased to 2.73% on the twenty-first day. The value never dropped below 2%, and the average was 2.36% in the whole aging period.

Chart 8 illustrates the ultrasonic wave velocity difference in the cylindrical shape. Contrary to what happened in the cubic molds, the difference between the CN and CBa3 compositions was high in the cylinders. This difference can be due to the surface roughness in cylindrical samples. On the first day, the difference was 2.09%, and it gradually increased to 5.40% on the twenty-first day. The average difference for these two compositions was 4.24%.

Although the maximum difference between the CBa3 and CBa6 compositions in cubic shapes was 2.52%, this value in the cylindrical shapes was 1.09%. It means, contrary to the cubic sample results, the difference of ultrasonic wave velocity for these two compositions with cylindrical geometry was not remarkable as the average difference value was 0.43%. Lowering the difference in cylindrical shapes can be due to the error in length measurement as the samples were cut and polished manually. So, the changes in length has a direct effect on UWV.

Meanwhile, the difference between the CN and CBa6 compositions in the cylindrical shapes was almost two times higher than values in the cubic shapes. The difference

increased over time and started from 3.20% on the first day and ended at 5.61% on the twenty-first day. The average difference was 4.68% that was twice more than 2.36% in cubic shapes.

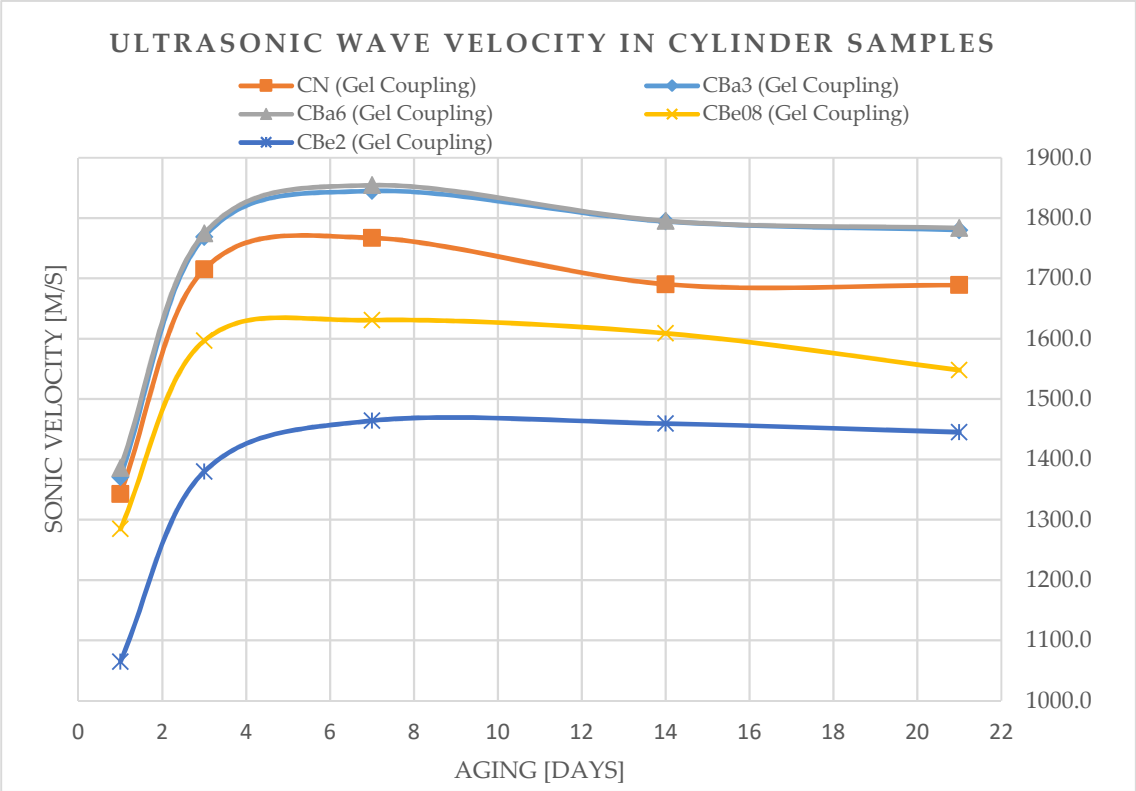

Chart 8 - Ultrasonic Wave Velocity in Cylinder Samples

• Role of Bentonite

Bentonite was added as an extender to reduce the density of cement samples to gain a broader range of density for finding the correlation between UCS and ultrasonic wave velocity by using piezoelements. Hence, the last two compositions, CBe08 and CBe2, were made for this purpose. As the water-to-cement ratio in these two compositions was different, 53.9% in CBe08 and 69.9% in CBe2, it should be noted that the difference in measurements was not only related to the role of bentonite. As the barite percentage was lower in CBe08, so this composition was selected as the baseline.

In cube samples, there was a significant difference between ultrasonic wave velocity in CBe08 and CBe2. In fact, the difference was -18.91% on the first day. The negative sign showed that CBe2 had less wave velocity than CBe08; 1162.1 m/s for CBe2 and 1343.6 m/s for CBe08. However, the difference rate decreased gradually and reached -12.94% on the last day of measurement, day twenty-first. The average difference in ultrasonic velocity measurements for all five days was -14.80%.

Same as the cubic samples, the difference in ultrasonic measurements was always decreasing in the cylindrical ones. It started with -17.11% on the first day and finished with -6.65% differences on the final day. The decreasing rate was sharper than measured in cubic samples due to changing the transmitter piezoelement sensor on day fourteenth. Due to this fact, the average difference value was -11.37% that was also less than the average in cubic samples.

• Role of Water

To investigate the impact of water in ultrasonic wave propagation velocity, at least three compositions with different water percentages were required. As the neat cement, 0.8% bentonite and 2% bentonite cement had different water-to-cement ratios with 44%, 53.9%, and 69.9%, respectively, these compositions were chosen to find the role of water. But the effect was not limited to water as CN had no bentonite while CBe08 and CBe2 had it.

As CBe2 had the highest water-to-cement ratio, so it was chosen as the baseline composition in this comparison. The minimum recorded value for velocity in the cubic shape's CN was 1301.6 m/s while it was 1162.1 m/s and 942.4 m/s for CBe08 and CBe2 in the same aging time. It means the difference between CN and CBe2 was 38.12% and between CBe08 and CBe2 was 23.31%. The positive value means that the compared position had higher velocity than baseline composition (CBe2). The difference in ultrasonic velocity in both comparisons (CN/CBe2 and CBe08/CBe2) had a decreasing trend. On day twenty-first, the CN velocity was 1813.65 m/s, the CBe08 velocity was 1678.9 m/s, while the CBe2 had 1461.67 m/s. It means the CN velocity was 24.08% higher than CBe2 velocity and the CBe08 velocity was 14.87% higher than CBe2. The average difference between CN and CBe2 in the whole five days of measurements was 29.84%, while it was 17.46% between CBe08 and CBe2.

The result of the analysis in cylindrical shape was the same as the cubic ones. The maximum difference between CN and CBe2 happened on the first day of measurement, 1342.9 m/s, and 1064.9 m/s, which means the difference was 26.10%, and the wave velocity for CBe08 was 1284.7 m/s on the same day, which represents 20.64% higher than CBe2. By passing the time, the velocity difference was decreasing, and on day twenty-first, the difference between CN and CBe2 was 16.87%, while it was 7.12% in CBe08/CBe2. In general, the average difference was 20.67% and 13.02% for CN/CBe2 and CBe08/CBe2, respectively.

• Role of Glass Bubble

The glass bubble impact was compared and checked with 2% bentonite cement, CBe2. The reason was that both compositions had almost the same water-to-cement ratios; 73.1% for C3M and 69.9% for CBe2. Although, the cement density was not equal; 10.9 ppg for C3M and CBe2 had 13.8 ppg.

As shown in Chart 7, the ultrasonic wave velocity of C3M (green line) was always higher than CBe2 (blue line) despite having a lower density and higher water-to-cement ratio. On the first day, C3M had 943 m/s, and CBe2 had 942.4 m/s velocity that means the difference was not considerable. Interestingly, the rate of difference became higher by passing days. On day twenty-first, the velocity of C3M was 1553.88 m/s while 1461.67 m/s for CBe2. It means the difference rate increased to 6.31%. This was precisely the opposite of what happened in other materials. The average difference between C3M and CBe2 compositions for ultrasonic wave velocity was 4.54% in five days of measurements. It should be noted that C3M was only made in cubic shape.

5.2.3 Compressive Strength Development

The second mechanical property investigated in this thesis was compressive strength. After performing NDT experiments, the cubic cement samples were placed into the UCS machine for the destructive test that gave the compressive strength value as a result. The impact of each additive on the compressive strength development is explained as follows:

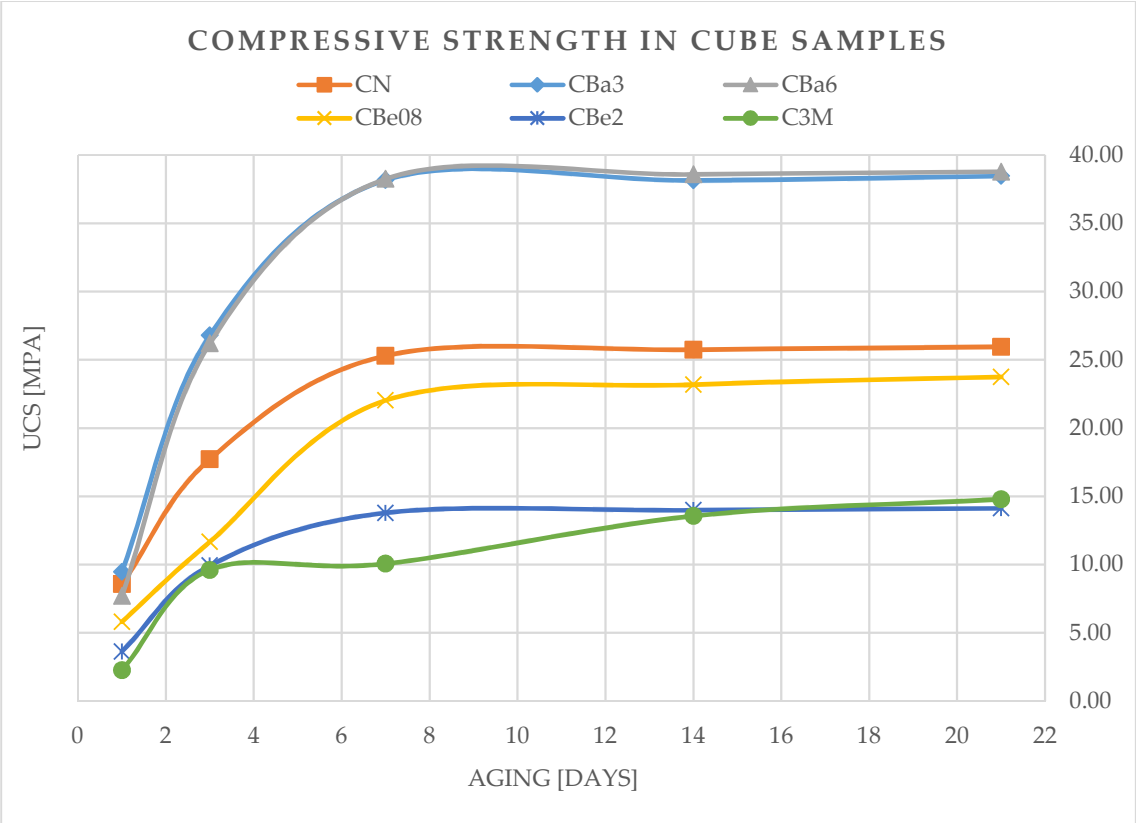

Chart 9 - Compressive Strength in Cube Samples

- Role of Barite

The barite's role in CBa3 and CBa6 was checked compared to the neat cement as all three mentioned compositions had the same water-to-cement ratios, 44%. As it is illustrated in Chart 9, all three compositions had almost the same UCS value on the first day; 8.57 MPa for CB, 9.46 MPa for CBa3, and 7.69 MPa for CBa6. Considering the CN as the baseline cement for comparison, the difference between CB and CBa3 was 10.34% and for CB and CBa6 was -10.26%. The negative value showed that CBa6 had interestingly lower UCS than CB on the first day. In addition, the six percent barite composition had an 18.68% UCS value lower than the three percent barite one on the first day.

A striking change is seen in the UCS values after the third day. The difference between CN and CBa3 became 51.30%. Contrary to the first day's values, CBa6 had a higher difference compressive strength than CN, 47.95%, on the third day, as predicted. However, the compressive strength of CBa6 was still below CBa3's value but not considerable, 2.21%. Moreover, considering the difference between CN and CBa3 and CBa6 in the rest of the days showed that no considerable change happened among the samples. On day fourteen, CBa3 to CN was 50.89%, while it became 48.15% on the final

day. CBa6 and CN differences were almost the same; 51.19% on the fourteenth day and 49.47% on the twenty-first day. The only observed change was that after day fourteen, the compressive strength value of CBa6 became higher than CBa3's value, although it was not considerable, by a maximum of 1.16%.

• Role of Bentonite

The CBe08 and CBe2 were compared together to find out the role of bentonite in compressive strength development. The composition with lesser bentonite always had a considerably higher value than the composition with higher bentonite. The reason is that bentonite develops the pore space within a oil well cement structure that causes decreasing the compressive strength (Jie Luo et al., 2019). On the first day of measurement, CBe08 had 5.81 MPa while the CBe2's USC was 3.63 MPa that showed a 60.15% difference. On the seventh and fourteenth days, UCS differences were almost the same as the first day; 59.75% and 65.79%. The maximum UCS value for both compositions was observed on the twenty-first day, where 23.75 MPa was for CBe08 and 14.12 MPa for CBe2. Once again, CBe08 had 68.18% higher compressive strength than CBe2. In total, the average UCS difference between these two compositions was 63.74%.

• Role of Water

Like the ultrasonic velocity comparison, the role of water in the compressive strength was investigated by checking the UCS development in CN, CBe08, and CBe2 due to their different W/C ratios.

Among these three compositions, the one with the highest water-to-cement ratio, CBe2 with 69.9%, had the lowest compressive strength since the first day of measurement. The recorded compressive strength for CBe2 was 3.63 MPa while 5.81 for CBe08 and 8.57 for CN. It means that CBe2's UCS value was 136.18% below CN, and CBe08 also had a 47.48% value less than CN on the first day.

Comparing values between CBe2 and CN showed that the difference was never fell below 78%. On the third day, the difference became 78.46%, and for the rest of the measurement days, the difference stayed almost constant at 83%. On the other hand, the difference between CBe08 and CN had a significant change and decreased to 14.84% on the seventh day. Since then, the difference trend gradually fell and reached 9.26% on the twenty-first day.

The average difference between CBe2 and CN was 93.19%, and the difference rate decreased since the third day, while for CBe08 and CN, the average value was 26.90% and the difference rate became slower day seventh.

• Role of Glass Bubble

Except for the first day, the glass bubble had almost the same effect in the compressive strength compared to two percent bentonite cement, although their density was not the same. Glass bubble had 10.9 ppg while CBe2 was a denser slurry, 13.8 ppg.

The difference between the two compositions was 60.38% on the first day. It means CBe2 with 3.63 MPa was more capable of withstanding against load than C3M with 2.62 MPa. On the third day, a sharp increase in the ultrasonic value was seen in C3M, and the difference decreased to only 3.26%. However, the seventh day measurement showed a

difference of about 37.03% that could be an error during measurement. The reason is that the difference in compressive strength was again back to 3.12% on the fourteenth day. Finally, the compressive strength of C3M became higher than CBe2 by 4.48% on the final day. It means that C3M had 14.79 MPa while 14.12 MPa was for CBe2 on the twenty-first day.

5.2.4 Overall Discussion

The ultrasonic wave velocity always shows a higher value with gel-coupling measurement rather than air-coupling since the coupling provides a better probe-surface contact leading to less ultrasonic wave attenuation which in turn transfers more energy into the sample. Although the difference is not considerable and the highest difference value is 2.34%, that can change the transmitter sensor. Based on the result, the difference is always higher at earlier aging days and decreased over time, regardless of water- and additive-to-cement ratio and density. It means only the aging day impacts the difference of gel and air-coupling ultrasonic wave velocities.

Barite, as a heavyweight agent, decreased the transit time that caused increasing the ultrasonic wave velocity. Using more amount of barite in the cement made moving the ultrasonic wave faster. However, the rate of ultrasonic velocity development was decreased with barite. The reason is that the cement microstructures are mainly formed in first seven days of curing (Ahmad et al., 2019). In the neat cement sample that had no additive, the ultrasonic wave developed almost 70% on the third day of measurements, while at the same time, this value was 69.81% for CBa3 and 61.51% for CBa6. In addition, the development value on the seventh day was 87.51% for CN; meanwhile, it was 87.20% for CBa3 and 85.82% for CBa6. It means that barite increased the ultrasonic wave velocity but decreased the ultrasonic velocity development.

Regarding barite's role for compressive strength development, the result represented that barite significantly increased compressive strength which is owing to reduce porosity and permeability in accordance to research performed by Ahmed and his colleagues (Ahmad et al., 2019). The maximum compressive strength measured for CN, CBa3, and CBa6 were respectively 25.95 MPa, 38.46 MPa, and 38.79 MPa on the twenty-first day that showed the barite's role. In addition, barite increased the UCS development, as well. For barite compositions samples, CBa3 and CBa6, the UCS was developed almost 99% on the seventh day, while it was 96.26% for the neat cement.

On the other hand, bentonite had the opposite effect compared to barite in terms of the ultrasonic wave velocity, as predicted. Adding more bentonite resulted in a significant dropping in the wave velocity. The main reason could be that more water is also required for using more bentonite in the slurry. So it should be noted that this significant dropping was related to bentonite itself, but also water-to-cement ratio affected the results. However, in the wave velocity development, bentonite played a similar role to barite. Lesser bentonite in the slurry was the reason for faster ultrasonic wave velocity development. In CBe08, 52.91% of velocity was developed within the first three days, while the velocity developed was 521.12% in CBe2. There was no change on the seventh day as well; the CBe08 still had a higher value than CBe2 for the wave velocity developments, 86.21%, and 85.15%.

Comparing the bentonite results with the neat cement for the compressive strength showed that the bentonite decreased compressive strength. The maximum compressive strengths that bentonite compositions reached were 23.75 MPa for CBe08 and 14.12 MPa for CBe2, which were below the CN's value. So it means adding more bentonite to a composition decreased its compressive strength. Contrary to the ultrasonic wave velocity development, bentonite increased the UCS development. 96.84% of the compressive strength was developed in CBe2 by day seventh, while only 90.41% was developed in CBe08 at the same time. However, the difference became less on day fourteenth, 98.68% for CBe2 and 96.84% for CBe08.

In this thesis, the compared compositions for the role of water (CN, CBe08, and CBe2) had different water-to-cement ratios as well as additive percentages. The difference in additive could cause uncertainty in recognizing the role of water. In general, higher ultrasonic velocity is a result of a higher water-to-cement ratio (Park et al., 2019), while the experiment's results showed that the wave velocity was decreased in higher water-to-cement ratio compositions. On the other hand, the previous study shows that a higher water content lowers the compressive strength in concrete (Li, 2004). The values gained from the experiments proved that. The highest water-to-cement ratio belonged to C3M, which had the lowest compressive strength among the six compositions on the fourteenth day. Only on the last day, the CBe2, which ranked as the second-highest water content composition with 69.90%, had a lower value than C3M, but the difference was not considerable, 4.48%.

The reason for using the glass bubble was to lighten the cement density and compare its role with bentonite as another lightweight additive. Although there was a significant difference between C3M and CBe2's densities, the ultrasonic velocity of the C3M was higher than CBe2, which can be an effect of more water content in this composition. Meanwhile, the compressive strength of both materials was almost the same at different aging periods, and on the final day of measurement, the C3M's compressive strength became even higher than CBe2. In general, the glass bubble composition had a lighter weight, but almost the same compressive strength and higher ultrasonic velocity compare to bentonite.

5.3 Correlation and Modeling

All data extracted from the experiments are plotted in different charts in order to exhibit the correlation among them the correlations and modeling are done by MATLAB software.

5.3.1 UCS Vs. Density

Chart 10 shows the uniaxial compressive strength versus density at all five days aging period. In a previous study done by Shohana Iffat, the model between UCS and density was linear (Iffat, 2016). However, the data follows an exponential behaviour in this thesis.

The model is

$$\boldsymbol{UCS = ae^{b.\rho} + ce^{d.\rho}}$$

Where ρ is the density of slurry measured in ppg,

Age	Variables in the model				$ae^{b\times 10.9}$	Intercept [MPa]	R^2
[day]	a	b	c	d	-	-	
1st	0	-3.146	0.04701	0.3271	1.662	2.26	0.9195
3rd	2.44E-14	2.138	8.668	0.009446	9.608	9.61	0.9646
7th	2.30E-15	2.285	1.862	0.1529	9.858	10.06	0.9456
14th	6.39E-15	2.227	5.072	0.08619	12.978	13.56	0.9277
21st	8.43E-15	2.211	6.739	0.0678	14.110	14.79	0.9163

Table 5 - Coefficients for UCS Vs. Density Model

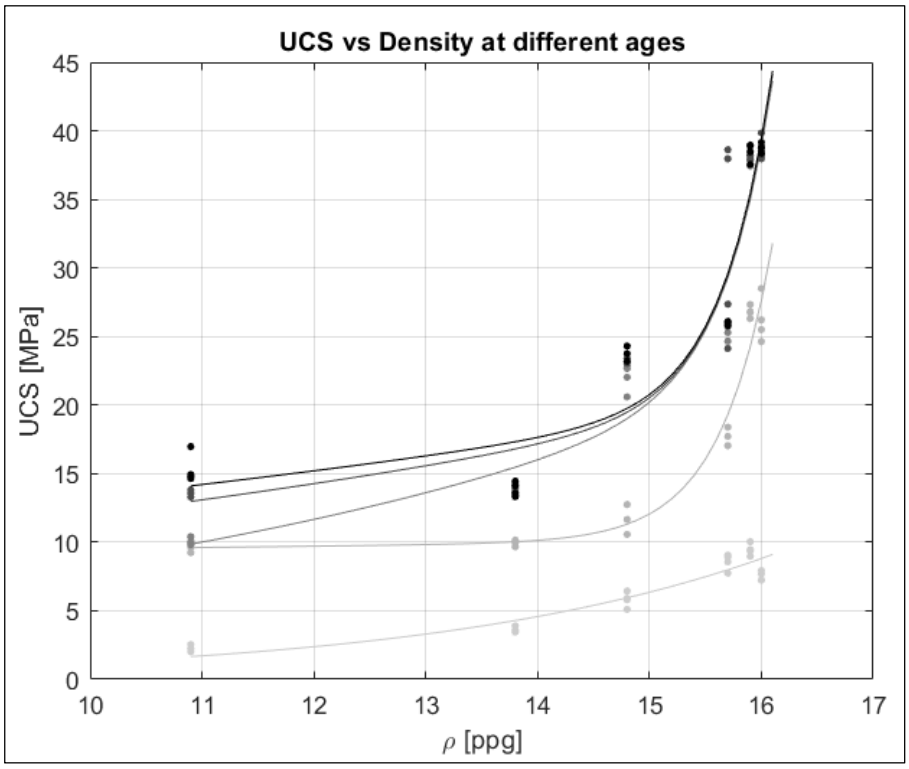

Chart 10 - UCS Vs. Density at Different Ages

As can be seen in Chart 10, the first term $ae^{b\times 10.9}$ describes the intercept and the second term describes $ce^{d.\rho}$ the curvature.

A more detailed analysis of Chart 10 shows the role of water content. In the density range between 14.8 to 16.0 ppg, slurries have a water-to-cement ratio of up to 54%, and the lines are more curved. Therefore, lowering the water content in the slurry makes the line more curved, while increasing the water-to-cement ratio causes the lines straighter.

5.3.2 UCS Vs. UWV

The compressive strength and the ultrasonic wave velocity are figured in Chart 11. Referring to previous studies, both exponential (Ramazan Demirboğa et al., 2004 & Hong

et al., 2020) and linear behaviors (Jamshidi et al., 2018 & Estévez et al., 2020) are modeled for UCS vs. UWV. Comparing the regression values for both behaviors in our models led us to choose the linear one as a model for our case.

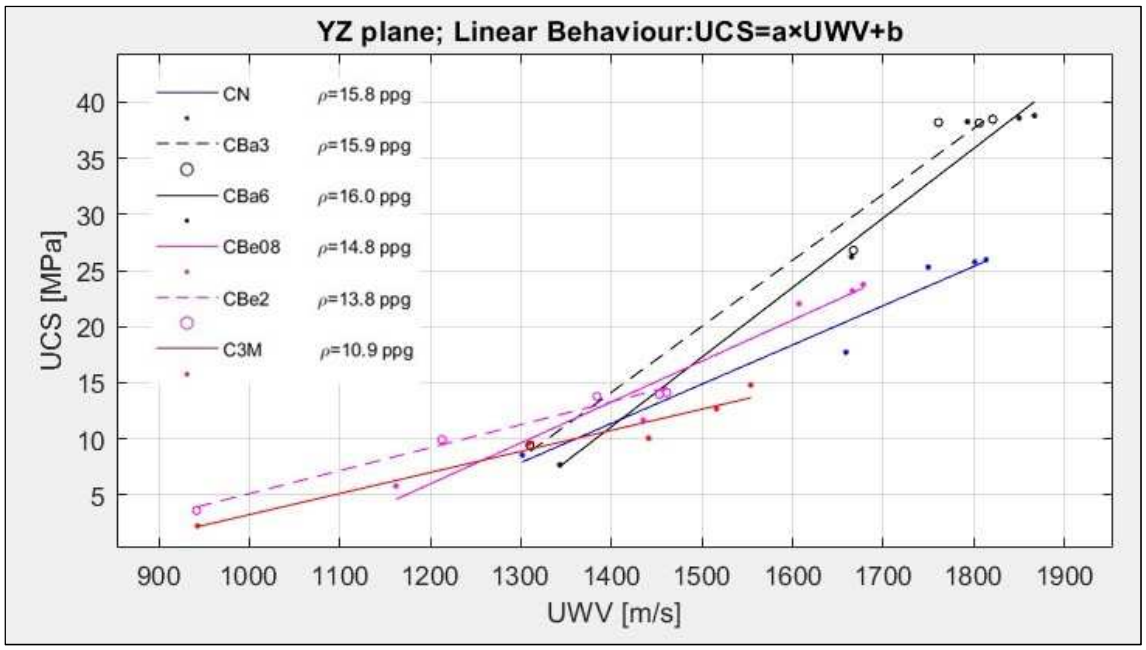

Chart 11 - UCS Vs. UWV with Different Densities

The linear model is

$$\boldsymbol{UCS = a.UWV + b}$$

In the following table, the coefficient for the respective compositions in the model is found. Mathematically speaking, they look fairly accurate, considering the error margin in these types of experimental work (Estévez et al., 2020). UWV is the ultrasonic wave velocity [m/s] that the researcher should measure and use in the model.

Cement Code	Linear Behavior $UCS = a.UWV + b$		
	a	b	R^2
CN	0.03493	-37.51	0.9533
CBa3	0.05878	-68.13	0.9721
CBa6	0.06193	-75.6	0.9846
CBe08	0.03647	-37.76	0.9564
CBe2	0.02049	-15.36	0.984
C3M	0.01879	-15.53	0.9572

Table 6 - Coefficients for UCS Vs. UWV Model

5.3.3 UCS Vs. Age

Although in some literature, a logarithmic behavior is modeled for UCS Vs. Age (Elaty, 2013), the experiment's results show that the power law model matches well with the data set as illustrated in Chart 12.

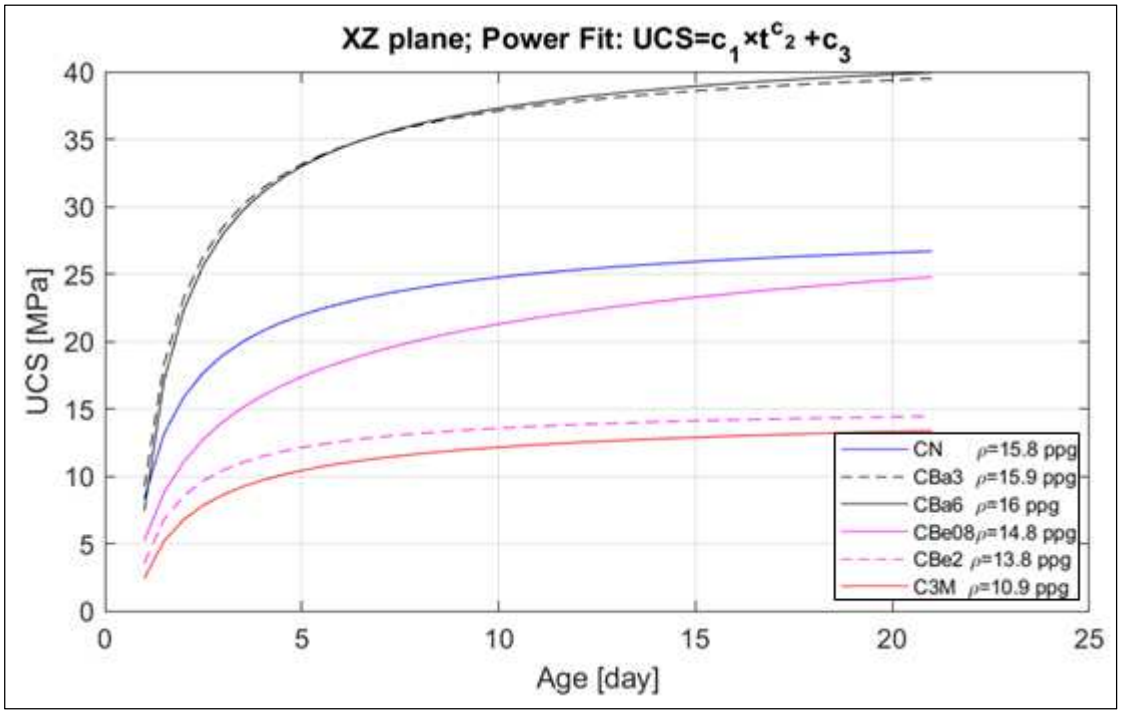

Chart 12 - UCS Vs. Age with Different Densities

The power law model for UCS Vs. Age is

$$\boldsymbol{UCS = c_1 \times t^{c_2} + c_3}$$

Where t is the aging period [day], and the coefficients are shown in the table below:

Cement Code	Power Law $UCS = c_1 \times t^{c_2} + c_3$			
	C_1	C_2	C_3	R^2
CN	-21.69	-0.6142	30.05	0.9759
CBa3	-33.36	-0.7875	42.57	0.9808
CBa6	-35.97	-0.7726	43.4	0.9824
CBe08	-36.75	-0.2491	42.01	0.9458
CBe2	-12.04	-0.7766	15.59	0.9861
C3M	-13.26	-0.5751	15.69	0.9484

Table 7 - Coefficients for UCS Vs. Age Model

5.3.4 UWV Vs. Age

Similar to UCS Vs. Age, the UWV Vs. Age model is a power law as well. However, both logarithmic and power law are applicable for this data set, but the power law is selected because of better regression value.

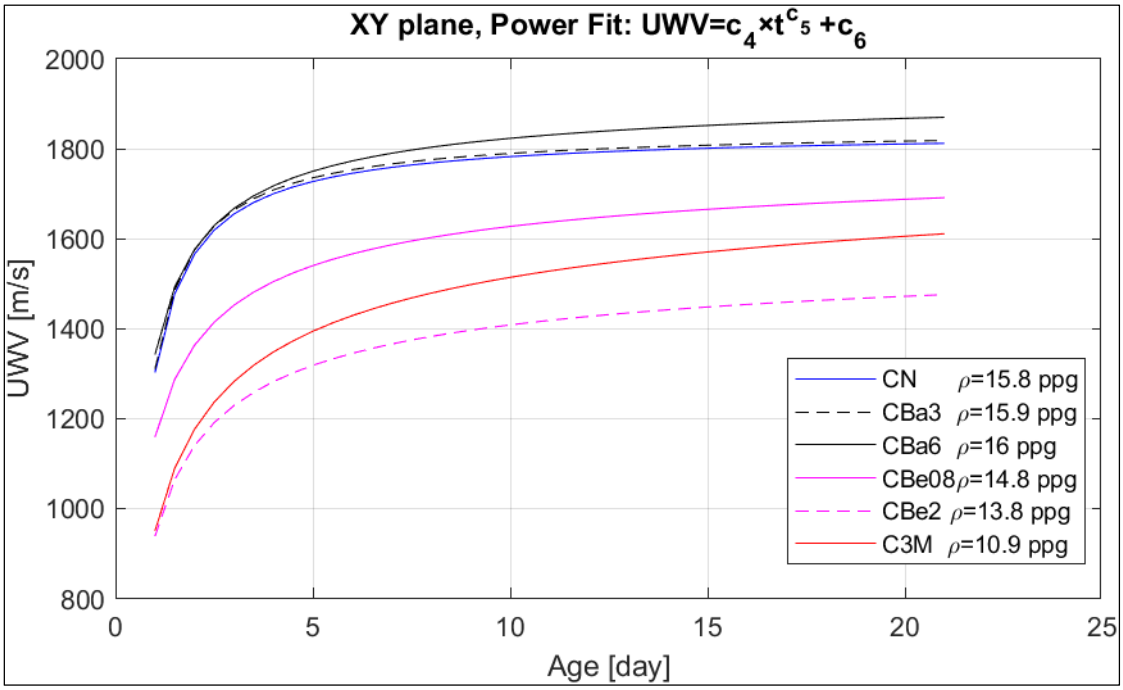

Chart 13 - UWV Vs. Age with Different Densities

The model for UWV Vs. Age is

$$\boldsymbol{UWV = c_4 \times t^{c_5} + c_6}$$

Where t is the aging period [day], and the coefficients are mentioned in Table 8

Cement Code	Power Law $UCS = c_4 \times t^{c_5} + c_6$			
	C_4	C_5	C_6	R^2
CN	-537.6	-0.9703	1840	0.9994
CBa3	-534.9	-0.9847	1845	0.9997
CBa6	-593.6	-0.721	1936	0.9998
CBe08	-665.3	-0.5292	1824	0.995
CBe2	-686.8	-0.501	1625	0.9952
C3M	-698	-0.6574	1643	0.9995

Table 8 - Coefficients for UWV Vs. Age Model

5.3.5 3D Model

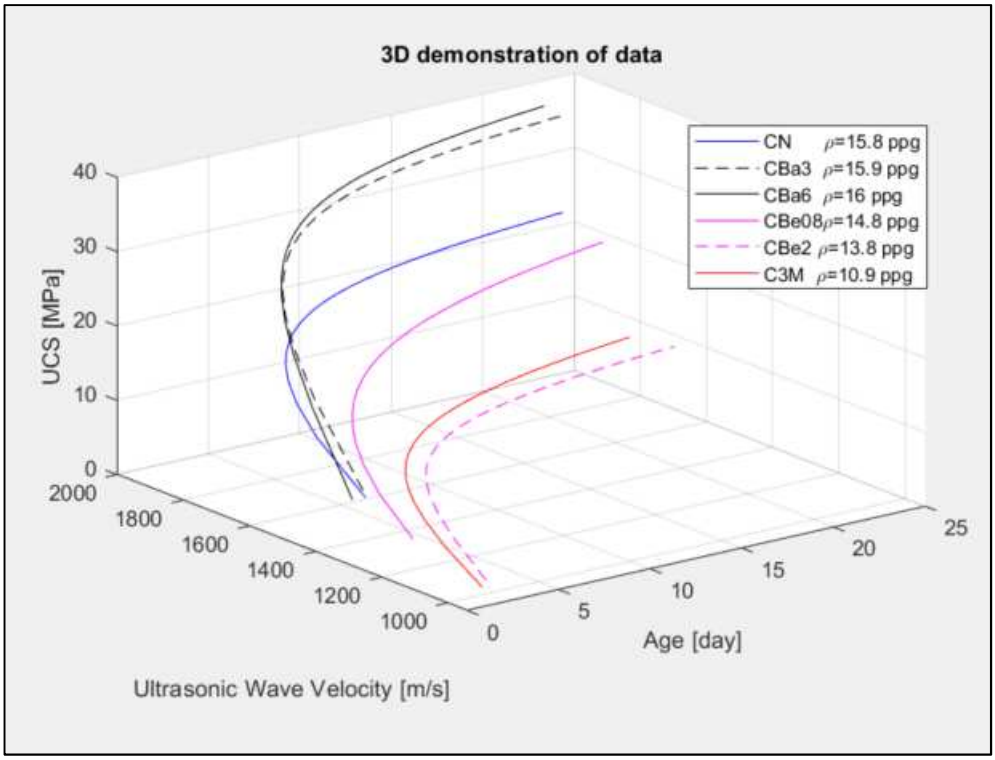

Assuming that the previous one-variable (time) models reflect the 3D curve on different plains (XZ, YZ, XY). We can merge these one-variable functions to get a two-variable model. The generated function has the form of z=f(x,y) with z, y, and x being respectively the UCS, UWV, and time. Time is the independent variable here.

$$\begin{cases} XZ\ reflection: UCS = c_1.t^{c_2} + c_3 \\ XY\ reflection: UWV = c_4.t^{c_5} + c_6 \\ YZ\ reflection: UCS = a.UWV + b \end{cases} \rightarrow UCS = \frac{f(time) + f(UWV)}{2}$$

$$\rightarrow \qquad UCS = \frac{[c_1.t^{c_2} + c_3] + a.UWV + b}{2} \rightarrow \boxed{UCS = \frac{[c_1.t^{c_2} + c_3] + a[c_4.t^{c_5} + c_6] + b}{2}} \quad *$$

What the highlighted function can currently do, is to get the time, then calculate the UCS directly through XZ reflection and indirectly through XY reflection. It then delivers an arithmetic average of them both.

An example of using this function is as follows:

We need the UCS estimation for a specific density (cement slurry recipe); let's choose C3M (The glass bubble additive). The variables a, b, and c_i will be selected based on tables 6, 7, and 8.

The estimated values for the 1st, 7th, and 21st days are respectively 2.37 MPa, 11.60 MPa, and 14.06 MPa with their measured counterparts as 2.26 MPa, 10.06 MPa, and 14.80 MPa.

• Although the function is reasonably accurate, it is still not what we deemed to get since the user should change the coefficients based on the slurry density every time. Moreover, s/he cannot use the UWV directly. That is why a regression technique was used to

develop the following **generic function** with independent inputs of density ($\rho[ppg]$), time (t[day]) and ultrasonic velocity (UWV[m/s]) and the output of UCS in [MPa]:

$$\overset{*}{\rightarrow} UCS = \frac{[c_1.t^{c_2} + c_3] + a.UWV + b}{2} = \frac{f_1(\rho).t^{f_2(\rho)} + f_a(\rho) \times UVW + f_3(\rho) + f_b(\rho)}{2}$$

Simpler form:

$$UCS = \left(\frac{f_a(\rho)}{2}\right)[\frac{f_1(\rho)}{f_a(\rho)}.t^{f_2(\rho)} + UWV + \frac{f_3(\rho) + f_b(\rho)}{f_a(\rho)}] \rightarrow UCS = C_0.(C_1.t^{f_2(\rho)} + UWV) + C_2$$

It is prudent to notice that the generic function is developed based on our data set. Hence it gives the best results only if the curing conditions and the slurry recipe match that of this thesis. Further data acquisition and processing could be employed to extend the application of this function to other curing conditions and slurry formulation. We should be careful, however, not to stretch its application over the point of validity.

Since the $f_i(\rho)$ functions are purely mathematical fit; we can use n-1 degree polynomial or any other suitable model to precisely fit the n number of points. However, this will come with the price that the model is only accurate for the specified densities. Reducing the degree of polynomial fit will stretch the model's validity over a broader range of densities with lower accuracy. This can be seen in Chart 14.

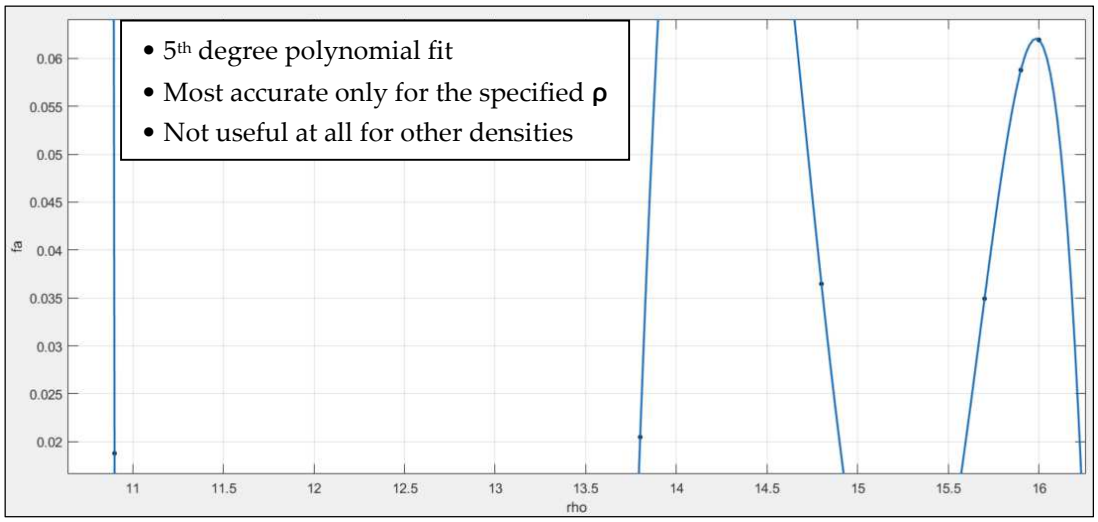

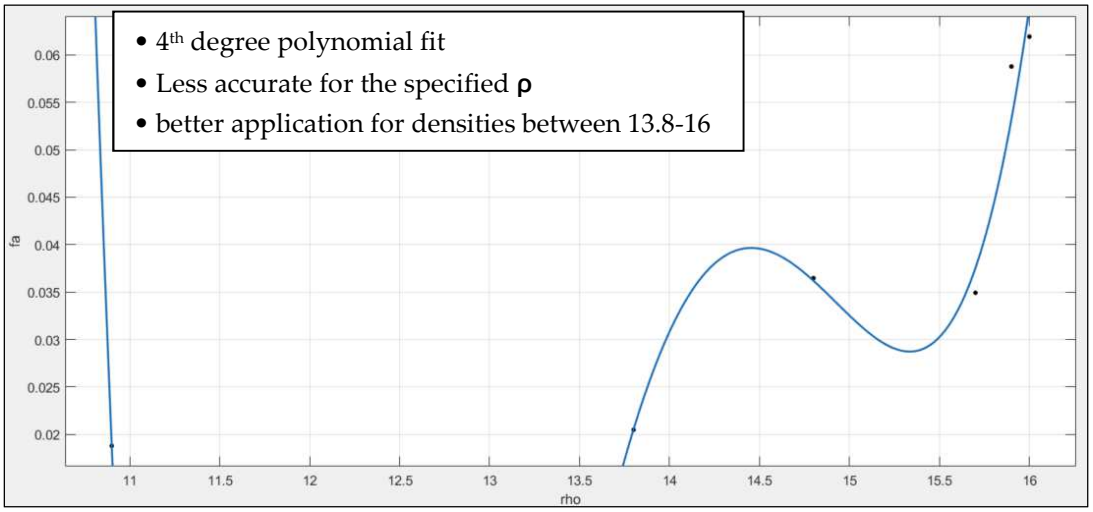

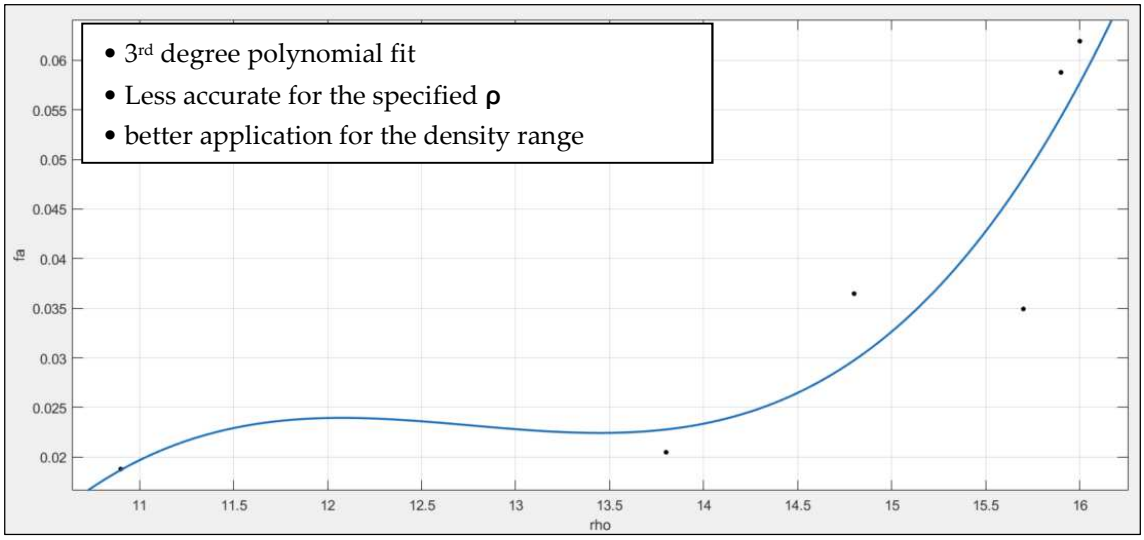

Chart 14 - The Accuracy Vs. Validity of the Model for Different Degree Polynomial

The generic function coefficients can be seen in the following table

Function	$f_i = p_1\rho^3 + p_2\rho^2 + p_3\rho + p_4$					Density range
	Polynomial coefficients				Accuracy	
	p_1	p_2	p_3	p_4	R^2	
f_a	0.001169	-0.04473	0.569	-2.382	0.84	10.8-16
f_b	-1.6399	62.4843	-790.6344	3302.5	0.86	10.8-16
f_1	0	-.8558	18.94	-117.40	0.55	10.8-16
f_3	0	1.225	-27.65	170.8	0.69	10.8-16
Function form: $f_2 = p_1.\sin^2(p_2.\rho) + p_3.\cos^8(p_4.\rho)$						
f_2	-0.8515	0.5943	-4.865	0.3535	0.77	10.8-16

Table 9 - Function coefficients for the 3D Model

Chapter 6 Conclusion

6.1 The Project Recap

Cement quality is one of the most significant parameters for maintaining an oil or gas integrity well. The project's primary purpose was to find a correlation between the ultrasonic wave velocity and the compressive strength to assess the oil well cement through a non-destructive method.

In this regard, sets of cement samples with different densities, water, and cement contents, and additive-to-cement ratios were designed and made to find a more general and precise correlation between UCS and UWV. The ultrasonic wave velocity was measured by piezo elements for each composition in cubic and cylindrical shapes in five different aging days. At the end of each UWV test, the tested cement sample was destroyed to acquire its compressive strength.

Eventually, data gathered during and after non-destructive and destructive tests were modeled with MATLAB software. 2D correlations between UCS and density, UCS and UWV, UCS and Age, and UWV and Age were found, and then a 3D model was made. Furthermore, a generic function with density, aging periods, and UWV as inputs and UCS value as output was developed.

6.2 Overall Conclusion

Curing time and condition directly affect microstructural changes inside the cement (Estévez et al., 2020). Consequently, passing the time makes the cement denser and lowers the volume of void spaces in the cement's internal structure (Iffat, 2016). The velocity of the ultrasonic wave is affected by the medium where the waves travel. More interconnected microstructures make the solid phase stronger and lower the void space which eventually, leads to a shorter transit time (Ye et al., 2001). Therefore, both compressive strength and ultrasonic wave velocity would be increased over time.

On the other hand, the result shows that barite increases the ultrasonic wave velocity. It means using more amount of barite in the slurry causes moving the ultrasonic wave faster and makes the cement sample stronger. The finding is matched with Kilincarslan's results (S. Kilincarslan et al., 2006).

As expected, bentonite compositions used in this research work lowers the ultrasonic wave velocity and compressive strength due to increasing the pore spaces inside the cement's structure (Jie Luo et al., 2019). Considering the bentonite compositions have different water-to-cement ratios, the result may be affected by water's role. Refer to a previous study, increasing bentonite content in the cement lowers the compressive strength in general (Noureddine Mesboua et al., 2018).

The experiment's results show a promising application for the enhanced lightweight slurry. While the glass bubble composition has a lower density than bentonites, it has almost the same compressive strength and higher ultrasonic wave velocity. So, it means that this material can be used as an ultra-lightweight material while having a less negative effect on the mechanical properties of the oil well cement.

6.3 Recommended Future Works

Some significant recommendations would improve the quality of the experiment and the results, consequently, as follows:

1) Curing the cement samples not only in the atmospheric condition but also in a wellbore condition.

2) Designing and comparing the slurries with the exact amount of specific additive, for example, water-to-cement ratio, in order to investigate the role of other additives, for instance, barite, more precisely.

3) Making more samples per composition that provides more data for the he correlations and modeling.

4) Preparing a wider density range by using more additives, especially the 3M Glass Bubble, to investigate more about its function and effect on cement's mechanical properties.

5) Comparing and finding a correlation between the ultrasonic wave velocities by piezo elements with the ultrasonic cement analyzer (UCA) unit.

6) Providing different suggestions rather than a direct linear relationship between UWV and UCS and a power law between UCS and Age period in order to find the best possible model between UCS and UWV.

7) Using machine learning methods for finding the correlations and making the models.

Bibliography

Agarwal, Anarag, and Jeffrey H. Lang. *Foundations of Analog and Digital Electronic Circuits*. Amsterdam: Elsevier, 2005.

Ahmed, Abdulmalek & Mahmoud, Ahmed Abdulhamid & Elkatatny, Salaheldin & Chen, Weiqing. (2019). The Effect of Weighting Materials on Oil-Well Cement Properties While Drilling Deep Wells. Sustainability. 11. 6776. https://doi.org/10.3390/su11236776.

Allan, M L. "Guidelines for Mixing and Placing Thermally Conductive Cementitious Grout (MIX 111)." | OSTI.GOV, December 14, 1999. https://www.osti.gov/servlets/purl/751159.

API RP 10B-2 standard (2010), *Recommended Practice for Testing Well Cements* (USA: API).

API Specification 10A (2010) *Specification for Cements and Materials for Well Cementing* (USA: API).

ASTM D2166-06 (2010), *Standard Test for Unconfined Compressive Strength of Cohesive Soil* (USA: ASTM International).

Basrawi, Marwan, and Danny Keck. "Nondestructive Testing Technologies for the Oil Industry." Paper presented at the Middle East Oil Show, Bahrain, June 2003. doi: https://doi.org/10.2118/81563-MS

Bergmann L (1957) Der Ultraschall und seine Anwendung in Wissenschaft und Technik — Nachtrag zum Literaturverzeichnis der 1954 erschienenen, 6th edn. S. Hirzel, Stuttgart

Chandler's Atmospheric Consistometer Model 1200 Instruction Manual, June 2018.

Chandler's Constant Speed Mixer Model 3260 Instruction Manual, July 2018.

Chiou, Chien-Ping & Margetan, Frank & McKillip, Matthew & Engle, Brady & Roberts, Ronald. (2016). Techniques and software tools for estimating ultrasonic signal-to-noise ratios. AIP Conference Proceedings. 1706. 070012. https://doi.org/10.1063/1.4940530.

Courland, Robert (2011). Concrete planet : the strange and fascinating story of the world's most common man-made material. Amherst, N.Y.: Prometheus Books. ISBN 978-1616144814. Retrieved 28 August 2015.

Elaty, Metwally. (2013). Compressive Strength prediction of Portland cement concrete with age using a new model. HBRC Journal. https://doi.org/10.1016/j.hbrcj.2013.09.005

Ensminger, Dale, and Leonard J. Bond. Ultrasonics Fundamentals, Technologies, and Applications. Boca Raton, FL: CRC Press, 2012.

Estévez, Esteban & Martín-Sánchez, Domingo & Argiz, Cristina & Sanjuán, Miguel. (2020). Ultrasonic Pulse Velocity—Compressive Strength Relationship for

Portland Cement Mortars Cured at Different Conditions. Crystals. 10. 133. https://doi.org/10.3390/cryst10020133.

Galdibini's Official Website, 2021. https://www.galdabini.eu/datasheets/quasar-200.

Glisson, Tildon H. Introduction to Circuit Analysis and Design. Springer, 2014.

Guner D, Ozturk H, Erkayaoglu M. Investigation of the elastic material properties of Class G cement. Structural Concrete. 2017; 18:84–91. https://doi.org/10.1002/suco.201600020

Haller, Kristian. Nonlinear Acoustics Applied to Nondestructive Testing. Karlskrona: Department of Mechanical Engineering, School of Engineering, Blekinge Institute of Technology, 2007.

Hong, Seonguk & Yoon, Sangki & Kim, Jonghyun & Lee, Changjong & Kim, Seunghun & Lee, Yongtaeg. (2020). Evaluation of Condition of Concrete Structures Using Ultrasonic Pulse Velocity Method. Applied Sciences. 10. 706. https://doi.org/10.3390/app10020706.

Ichim, Adonis. (2017). Experimental Determination of Oilfield Cement Properties And Their Influence On Well Integrity.

Iffat, Shohana. (2016). Relation Between Density and Compressive Strength of Hardened Concrete. CONCRETE RESEARCH LETTERS. 6. 182-189.

J.-K Kim, Y.-H Moon, S.-H Eo, Compressive strength development of concrete with different curing time and temperature, Cement and Concrete Research, Volume 28, Issue 12, 1998, Pages 1761-1773, ISSN 0008-8846, https://doi.org/10.1016/S0008-8846(98)00164-1

Jamshidi, A., Zamanian, H. & Zarei Sahamieh, R. The Effect of Density and Porosity on the Correlation Between Uniaxial Compressive Strength and P-wave Velocity. Rock Mech Rock Eng 51, 1279–1286 (2018). https://doi.org/10.1007/s00603-017-1379-8.

Jianfeng Zhang, Shenyu Li, Fu-Zhen Xuan, Fuqian Yang, Effect of plastic deformation on nonlinear ultrasonic response of austenitic stainless steel, Materials Science and Engineering: A, Volume 622, 2015, Pages 146-152, ISSN 0921-5093, https://doi.org/10.1016/j.msea.2014.10.082.

Jie Luo, Chuanchang Li, Yafei Ma, Lei Wang, Bentonite replacing part of cement concrete for resistance to chloride ion attack, E3S Web Conf. 136 03011 (2019), https://doi.org/10.1051/e3sconf/201913603011.

JPT staff, "Ultralight Hollow Glass Spheres Improve Cement Slurry Performance." J Pet Technol 55 (2003): 26–28. doi: https://doi.org/10.2118/0203-0026-JPT.

K.-H. Schwalbe, J.D. Landes, J. Heerens, 7.02 - Classical Fracture Mechanics Methods*, Editor(s): I. Milne, R.O. Ritchie, B. Karihaloo, Comprehensive Structural Integrity, Pergamon, 2007, Pages 3-42, ISBN 9780080437491, https://doi.org/10.1016/B0-08-043749-4/07043-9.

Kern's Official Website: https://www.kern-sohn.com/cgi-bin/cosmoshop/lshop.cgi?action=suche&ls=en&gesamt_zeilen=0&suchbegriff=FCB%203K0.1.

L. Ferrari, J. Kaufmann, F. Winnefeld, J. Plank, Reaction of clinker surfaces investigated with atomic force microscopy, Construction and Building Materials, Volume 35, 2012, Pages 92-96, ISSN 0950-0618, https://doi.org/10.1016/j.conbuildmat.2012.02.089.

Ladislav CARBOL, Ivo KUSÁK, Jan MARTINEK, and Petra VOJKUVKOVÁ. (2015) "Influence of Transducer Coupling in Ultrasonic Testing," n.d.

Li, G. The E_ect of Moisture Content on the Tensile Strength Properties of Concrete. Master's Thesis, University of Florida, Gainesville, FL, USA, 2004.

Li, Weibin & Cho, Younho & Li, Xianqiang. (2013). Comparative Study of Linear and Nonlinear Ultrasonic Techniques for Evaluation Thermal Damage of Tube-Like Structures. Journal of the Korean Society for Nondestructive Testing. 33. https://doi.org/10.7779/JKSNT.2013.33.1.1

Marc Jolin, Louis-Samuel Bolduc, Frederic Gagnon, Benoıt Bissonnette, and Dennis Burns (200). "UNDERSTANDING THE PUMPABILITY OF CONCRETE," 2009. https://dc.engconfintl.org/cgi/viewcontent.cgi?article=1009&context=shotcrete.

Marques, Aline & Paes, Brahmani & Marques, Eduardo Antonio & Pereira, Luana. (2015). Correlations between uniaxial Compressive strength and point load strength for some brazilian high-grade metamorphiC roCks. Revista Brasileira de Geologia de Engenharia. 4. 47.

Mason, W. P. 1950. Piezoelectric Crystals and Their Application to Ultrasonics. New York: Van Nostrand.

Mostavi, Amir & Tehrani, Niloofar & Kamali, Negar & Ozevin, Didem & Chi, Sheng-Wei & Indacochea, Ernesto. (2017). The application of water coupled nonlinear ultrasonics to quantify the dislocation density in aluminum 1100. AIP Conference Proceedings. 1806. 060003. https://doi.org/10.1063/1.4974612.

Munjal, Pankaj & Kian Hau, Kong & Prabhakar, Abhinav & Cheng, Arthur. (2019). Oil Well Cement for high temperature-A review. IOP Conference Series: Materials Science and Engineering. 652. 012055. https://iopscience.iop.org/article/10.1088/1757-899X/652/1/012055.

Nagy, Peter & Rose, James. (1993). Surface roughness and the ultrasonic detection of subsurface scatterers. Journal of Applied Physics. 73. 566 - 580. https://doi.org/10.1063/1.353366.

NASA Reliability Preferred Practices for Design and Test. Ultrasonic Testing of Aerospace Materials, Practice No. PT-TE-1422, 1999, https://extapps.ksc.nasa.gov/Reliability/Preferred_practices.html.

Naval Material Science and Engineering, EN380, Chapter 10: Deformation. United States Naval Academy. https://www.usna.edu/NAOE/academics/en380.php

Nelson, Erik B., and Dominique Guillot. Well Cementing. Sugar Land, TX: Schlumberger, 2006.

Norsok D-010 Standard. 2004. Well Integrity In Drilling and Well Operations. Norway Standards

Noureddine Mesboua, Khaled Benyounes & Abdelbaki Benmounah | Sanjay Kumar Shukla (Reviewing Editor) (2018) Study of the impact of bentonite on the physico-mechanical and flow properties of cement grout, Cogent Engineering, 5:1, https://doi.org/10.1080/23311916.2018.1446252

Pain, H. J. 1999. The Physics of Vibrations and Waves. 5th ed. Chichester: Wiley.

Parisa Shokouhi, Jacques Rivière, Colton R. Lake, Pierre-Yves Le Bas, T.J. Ulrich, Dynamic acousto-elastic testing of concrete with a coda-wave probe: comparison with standard linear and nonlinear ultrasonic techniques, Ultrasonics, Volume 81, 2017, Pages 59-65, ISSN 0041-624X, https://doi.org/10.1016/j.ultras.2017.05.010.

Park, Jong Y.; Yoon, Young G.; Oh, Tae K. 2019. "Prediction of Concrete Strength with P-, S-, R-Wave Velocities by Support Vector Machine (SVM) and Artificial Neural Network (ANN)" *Appl. Sci.* 9, no. 19: 4053. https://doi.org/10.3390/app9194053

Pasquale V. (2011) Curie Temperature. In: Gupta H.K. (eds) Encyclopedia of Solid Earth Geophysics. Encyclopedia of Earth Sciences Series. Springer, Dordrecht. https://doi.org/10.1007/978-90-481-8702-7_109.

Perez, Nicolás. (2008). Evaluation of air coupling ultrasonic transducers for surface roughness measurement. Revista Iberoamericana de sensores.

PI Ceramic GmbH Official Website, 2021 https://www.piceramic.com/en/products/piezoelectric-materials/

PiezoDrive's P200 V7 Power Amplifier Manual and Specification, 2020.

R.P.L. Nijssen, 2 - Phenomenological fatigue analysis and life modeling, In Woodhead Publishing Series in Composites Science and Engineering, Fatigue Life Prediction of Composites and Composite Structures, Woodhead Publishing, 2010, Pages 47-78, ISBN 9781845695255, https://doi.org/10.1533/9781845699796.1.47.

Ramazan Demirboğa, İbrahim Türkmen, Mehmet B. Karakoç. (2004). Relationship between ultrasonic velocity and compressive strength for high-volume mineral-admixtured concrete, Cement and Concrete Research, Volume 34, Issue 12, Pages 2329 - 2336, ISSN 0008 - 8846, https://doi.org/10.1016/j.cemconres.2004.04.017.

Rao, Prabhakar P., Sutton, David L., Childs, Jerry D., and Willis C. Cunningham. "An Ultrasonic Device for Nondestructive Testing of Oilwell Cements at Elevated Temperatures and Pressures." J Pet Technol 34 (1982): 2611–2616. doi: https://doi.org/10.2118/9283-PA

S. Kilincarslan, I. Akkurt, C. Basyigit, The effect of barite rate on some physical and mechanical properties of concrete, Materials Science and Engineering: A, Volume

424, Issues 1–2, 2006, Pages 83-86, ISSN 0921-5093, https://doi.org/10.1016/j.msea.2006.02.033.

Shin SW, Qureshi AR, Piezoelectric Lee JY, et al. Piezoelectric sensor based nondestructive active monitoring of strength gain in concrete. Smart Mater Struct 2008; 17:055002.

Sifatullah Bahij, Safiullah Omary, Francoise Feugeas, Amanullah Faqiri. Fresh and hardened properties of concrete containing different forms of plastic waste – A review, Waste Management, Volume 113, 2020, Pages 157-175, ISSN 0956-053X, https://doi.org/10.1016/j.wasman.2020.05.048

Singh, Sanjay K, Subekti, Herry , Al-Asmakh, Mona , and Layth Al-Samarraie. "An Integrated Approach to Well Integrity Evaluation via Reliability Assessment of Well Integrity Tools and Methods: Results from Dukhan Field, Qatar." Paper presented at the SPE International Production and Operations Conference & Exhibition, Doha, Qatar, May 2012. doi: https://doi.org/10.2118/156052-MS

Szabo TL, Wu J (2000) A model for longitudinal and shear wave propagation in viscoelastic media. J Acoust Soc Am 107(5): 2437–2446

Ultrasonic Nondestructive Evaluation Systems: Industrial Application Issues. Cham: Springer International Publishing AG, 2015.

Vignes, Birgit "Qualification of Well Barrier Elements - Test Medium, Test Temperatures and Long-Term Integrity." Paper presented at the SPE European Health, Safety and Environmental Conference in Oil and Gas Exploration and Production, Vienna, Austria, February 2011. doi: https://doi.org/10.2118/138465-MS

Wan Renpu, Chapter 5 - Production Casing and Cementing, Editor(s): Wan Renpu, Advanced Well Completion Engineering (Third Edition), Gulf Professional Publishing, 2011, Pages 221-294, ISBN 9780123858689, https://doi.org/10.1016/B978-0-12-385868-9.00009-9.

Wang, Mingnian & Hu, Yunpeng & Jiang, Cheng & Wang, Yicheng & Liu, Dagang & Tong, Jianjun. (2020). Mechanical Characteristics of Cement-Based Grouting Material in High-Geothermal Tunnel. Materials. 13. 1572. 10.3390/ma13071572.

Wang, Zhe & Cui, Ximing & Ma, Hongbao & Kang, Yihua & Deng, Zhiyang. (2018). Effect of Surface Roughness on Ultrasonic Testing of Back-Surface Micro-Cracks. Applied Sciences. 8. 1233. https://doi.org/10.3390/app8081233.

Ye, Guang & Breugel, Klaas & Fraaij, A.L.A.. (2001). Experimental study on ultrasonic pulse velocity evaluation of the microstructure of cementitious material at early age. HERON, vol. 46 (3), 2001. 46.

Acronyms

API	American Petroleum Industry
DAET	Dynamic Acousto-Elastic Testing
EMI	Electro-Mechanical Impedance
HPHT	High Pressure High Temperature
HSR	High Sulfate Resistant
MSR	Medium Sulfate Resistant
NDT	Non Destructive Test
NRUS	Non-linear Resonance Ultrasound Spectroscopy
PCF	Pound per Cubic Feet
PPG	Pound Per Gallon
PZT	Piezoelectric lead Zirconate Titanate
RPM	Revolution Per Minute
RUS	Resonance Ultrasound Spectroscopy
SP. GR.	Specific Gravity
UCA	Ultrasonic Cement Analyzer
UCS	Uniaxial Compressive Strength
UPV	Ultrasonic Compressional Wave Velocity
WBE	Well Barrier Element

Symbols

F	Applied Load	[N]
A	Area	[mm^2]
σ	Compressive Strength	[N/mm^2 or MPa]
ρ	Density	[ppg]
ε	Strain	Dimensionless
l_f	Final Length	[mm]
φ	Free-Fluid Percentage	Dimensionless
V_{FF}	Free-fluid Volume	[millilitre]
l_i	Initial Length	[mm]
M	Mass	[gr]
v_p	P-wave Velocity	[m/s]
v_d	Poisson's Ratio	Dimensionless
v_s	S-wave Velocity	[m/s]
V	Velocity	[m/s]
V	Volume	[millilitre]
E	Young Modulus	[N/mm^2 or MPa]

List of Figures

List of Tables

List of Charts